Lucia Salmeron Gallar

EVALUATION OF CHEST CT IMAGES OF COVID-19 PATIENTS TREATED WITH RADIOTHERAPY

Treball Fi de Grau

dirigit pel Dr. Pere Rafols

dirigit per la Dra. Meritxell Arenas

Grau en Enginyeria Biomèdica

UNIVERSITAT ROVIRA I VIRGILI

Tarragona

2021

Abstract

In the present final degree project, a computer program is developed in the Matlab® environment that serves as a tool to evaluate the evolution of the lung volume of COVID-19 patients treated with low-dose radiotherapy (LD-RT). Chest CT images from the study "LOW DOSE ANTI-INFLAMMATORY RADIOTHERAPY FOR THE TREATMENT OF COVID-19 PNEUMONIA: MULTI-CENTER PROSPECTIVE STUDY (IPACOVID)" carried out by the radiotherapy oncology department of the Sant Joan University Hospital, Reus.

The developed simulation software was then used to study, through segmentation, the development of lung volume during LD-RT treatment for its reduction of inflammation. For this, a series of simulations have been carried out, varying the generated algorithm to obtain exact volumes. Subsequently, these values have been compared with those expected by the Sant Joan University Hospital to see the correlation.

These results have helped to verify the correct operation of the program. In addition, it has been proven that there is a clear anti-inflammatory effect and that there are differences in the evolution depending on the characteristics of the patient.

The anti-inflammatory effects of LD-RT have been demonstrated in other experimental studies and it may be an alternative for patients with COVID-19 pneumonia.

Keywords: Radiotherapy, COVID-19, Volume, DICOM

Índex

Abbreviations 7

1 Introduction 8

1.1 Problem Description 8
1.2 Project Framework 9
1.2.1. Project Methodology 11
1.3 Objectives 11
1.4 Memory Guide 11

2 Theoretical Framework 12

2.1 Radiotherapy 12
2.1.1. Anti-Inflammatory Effects of Low Doses Radiotherapy (LD-RT) 12
2.2 Coronavirus 12
2.3 Computed Tomography (CT) 13
2.3.1. Chest CT 14
2.4 Medical imaging 15
2.4.1. Historical Foundation 15
2.4.2. Medical imaging processing 16
2.4.3. Key problemes 16

3 Materials 16

3.1 Software 16
3.2 Files 17
3.1.1. DICOM 17
3.1.2. Data 17

4. Methods 19

4.1. Collection of images 19
4.2. Modification and Classification 19
4.2.1. Modification 19
4.2.2. Classification 20
4.3. Image Processing Algorithms 21
4.3.1. 2D Volume calculation algorithm enhanced with information of the previous CT section 21
4.3.1.1. Main 21
4.3.1.2. Principal 21
4.3.1.3. Lung 24

4.3.1.4. Mask 28
4.3.2.Image Processing – 3D VOLUME 31
4.3.2.1. LUNG 31
4.4. Evaluation 33
5. Results 34
5.1. 2D-Algorithm with previous section 34
5.2. 3D-Algorithm 35
5.3. Clinic results 37
6. Conclusions and Future Lines 43
6.1. Conclusions 43
6.2. Future Lines 43
7. Annexes 44
7.1. Normal patient 44
7.2. Anormal TAC 54
Bibliography 56

Figures

Figure 1 - Classification of COVID-19 disease states and potential therapeutic targets. 10
Figure 2 - New Daily Global Confirmed COVID-19 Deaths 13
Figure 3 – Drawing of the patient on a table that slides through the CT machine 13
Figure 4 - DICOM file export screen as 3D files all in the same series 19
Figure 5 - General directory with the division of folders for each patient identified with their ID number 20
Figure 6 - Folder of a patient with its three DICOM files inside. Each one corresponding to the TACs that have been carried out 20
Figure 7 - Principal function flow chart 22
Figure 8 - Lung function flow chart 24
Figure 9 - Representation of the original 3D structure 25
Figure 10 - Central slide of our structure 26
Figure 11 - Mask for the central slide 26
Figure 12 - Mask for the next slide to the center 27
Figure 13 - Differences between the two masks previously calculated. 27
Figure 14 - Mask function flow chart 28
Figure 15 - Central slide with threshold valeu applied 29
Figure 16 - Central slide inverted 29
Figure 17 - Mask with imfill() 30
Figure 18 - Mask with imclearborder() 30
Figure 19 - Mask with imerode() 30
Figure 20 - Final mask 31
Figure 21 - Lung function flow chart 2D 32
Figure 22 - Final Volume with 3D algorithme 33
Figure 23 - Final Basal Volume Example with 2D algorithme 34
Figure 24 - Cross section of the structure represented in figure 23 35
Figure 25 - Longitudinal section of the structure represented in figure 23 35
Figure 26 - Final Basal Volume Example with 3D algorithme 36
Figure 27 - Cross section of the structure represented in figure 25 36
Figure 28 - Longitudinal section of the structure represented in figure 26 36
Figure 29 - Boxplot Specific Evolution 38
Figure 30 - Percentage Evolution Linear Plot 39
Figure 31 - Mean Percentage plot 40

Figure 32 - Mean Percentage plot divided by sex 40
Figure 33 - PAFi/Volume Scatter plot 41
Figure 34 - SAFi/Volume Scatter plot 42
Figure 35 - 3D Raw Structure 44
Figure 36 – Raw central cut and with its mask applied 44
Figure 37 - raw top cuts and with their masks applied 1/2 45
Figure 38 - raw top cuts and with their masks applied 2/2 45
Figure 39 - - raw top cuts and with their masks applied 2/2 46
Figure 40 - Undercuts raw and with their masks applied 1/4 48
Figure 41 - Undercuts raw and with their masks applied 2/4 49
Figure 42 - Undercuts raw and with their masks applied 3/4 50
Figure 43 - Undercuts raw and with their masks applied 4/4 51
Figure 44 - Basal, week and month volumes obtained 53
Figure 45 - Structure of the patient with abnormal CT 54
Figure 46 - CT central section of figure 44 54
Figure 47 - Lung volume obtained from the CT scan in Figure 44 55
Figure 48 - Example of cutting and applying your CT mask from figure 44 55

Tables

Table 1 – Clinical characteristics of patients with COVID-19 treated with low-dose radiation therapy 21

Table 2 – Table on the number of TACs and mean values of volumes, PAFi and SAFi.....40

Table 3 – Table of Quartile description 42

Table 4 – Causes of death, from COVID-19 or other causes following low-dose radiation therapy (LD-RT) 45

Table 5 – Data of the processing of the upper half of the TAC (slide, area, similarity with the previous slide) 50

Table 6 – Data of the processing of the lower half of the TAC (slide, area, similarity with the previous slide) 55

Abbreviations

HUSJR	Hospital Universitari Sant Joan de Reus
RT	Radiotherapy
LD-RT	Low-Doses Radiotherapy
CT	Computed tomography
WHO	World Health Organization
COVID-19	Coronavirus disease
SARS-CoV-2	Severe acute respiratory syndrome coronavirus 2
SARS	Severe acute respiratory syndrome
RNA	Ribonucleic acid
ALARA	As Low As Reasonably Achievable
SAFi	Ratio arterial oxygen saturation and isnpiration oxygen portion
PAFi	Ratio arterial pressure of oxygen and isnpiration oxygen portion

1 Introduction

1.1 Problem Description

The coronavirus disease (COVID-19) is a global pandemic caused by an acute respiratory syndrome. In early December 2019, the first cases of this disease were identified in Wuhan, China and identifying the severe acute respiratory syndrome coronavirus 2 (SARS-CoV-2) as the causative agent. These cases had a very high contagion rate. Since then, there has been a rapid spread of this RNA virus throughout the world, since it has a very high contagion rate, being recognized by the World Health Organization (WHO) as a pandemic on March 11, 2020. The consequences of the COVID-19 were quickly noticed in Spain since it is one of the countries where the infection has shown the most virulence. This has put our national health system under unimaginable stress and with evident risk of collapse as seen in the different waves of the pandemic.

COVID-19 is a respiratory disease caused by the coronavirus that produces significant morbidity and mortality. Symptoms are variable but often include fever, dry cough, sore throat, headache, fatigue, sputum, dyspnea, and loss of smell and taste. Some patients develop pneumonia that can lead to respiratory failure or SARS. According to Chinese experience, 81% of the clinical cases were mild in nature with an overall fatality rate of 2.3%, while a small subgroup of 5% suffered respiratory failure, septic shock, and multiple organ failure leading to death in half of these cases, suggesting that it is within this group that the opportunity to save lives exists if appropriate measures are taken [1].

There appear to be two distinct but overlapping disease subsets, the first caused by the virus itself and the second by the host response. In the first stage, patients will benefit from anti-virus drug therapy and the use of anti-inflammatory therapy may not be necessary and may even lead to viral replication. In the second stage of lung disease, viral multiplication and localized inflammation in the lung take place. During this stage, patients develop pneumonia, with a cough and fever. It is at this stage that most COVID-19 patients would need to be hospitalized for close observation and treatment. If hypoxia occurs, patients are likely to progress and require mechanical ventilation, and in that situation, the use of anti-inflammatory therapies, such as corticosteroids, could be helpful and could be used with caution. A minority of COVID-19 patients will progress to the third and most severe stage of the disease, manifesting as an extrapulmonary systemic hyperinflammation syndrome. In this stage, systemic inflammation markers will rise, and COVID-19 infection will cause a decrease in helper, suppressor, and regular T cells [2].

Due to the situation of our national health system, the effective management of patients with pneumonia and acute respiratory distress syndrome is of vital importance. Due to the lack of effective pharmacological concepts, this situation has generated interest in (re) considering historical reports on the treatment of patients with low-dose radiotherapy (LD-RT) for pneumonia. LD-RT can influence anti-inflammatory effects. The dose is less than 1% of the doses used for cancer treatment and ranges from 0.3 to 0.7 Gy. LD-RT has been used for more than a century in the treatment of pneumonia, especially interstitial and atypical.

In the review by Calabrese et al., LD-RT to the lungs were found to be associated with good response rates and resolution of symptoms. The authors reviewed 15 studies including 863 cases of pneumonia that were effectively treated with low-dose x-rays, improving symptoms, increasing cure, and reducing mortality [2]. The mechanism by which X-ray treatment acts on pneumonia involves the induction of an anti-inflammatory phenotype that leads to a rapid reversal of clinical symptoms, facilitating the resolution of the disease. Treatment was most effective when irradiation was administered 6 to 14 days after the clinical onset of the disease. After 14 days, the successful response rate decreased by approximately

50%. The authors' conclusion is that LD-RT offers excellent potential as a treatment for interstitial pneumonia, especially when used during the early stages of the disease [3].

1.2 Project Framework

COVID-19, also known as SARS-CoV-2, is an RNA virus that can cause severe acute respiratory illnesses, with severe lower respiratory tract infection followed by bronchitis, pneumonia, and fibrosis. Patients can develop pneumonia, which conditions severe respiratory failure, especially in the elderly and patients with low respiratory function and a picture of SARS in these patients.

In the pathogenesis of SARS, a cytokine storm occurs, involving the considerable release of pro-inflammatory substances. When the virus infects the upper and lower respiratory tract, it can cause mild or very acute respiratory syndrome with the consequent release of pro-inflammatory cytokines. Suppression of pro-inflammatory cytokines has been shown to have a therapeutic effect in many inflammatory diseases, including viral infections.

Currently, there is no drug capable of treating SARS-CoV-2, the only treatments are those aimed at treating the side effects caused by the virus, such as inflammation and pulmonary fibrosis, recognized as the first causes of death.

Radiotherapy (RT) has been used for more than a century in the treatment of pneumonias, especially interstitial and atypical ones. The mechanism by which X-ray treatment acts on pneumonia involves the induction of an anti-inflammatory phenotype that leads to a rapid reversal of clinical symptoms, facilitating the resolution of the disease [3]. Treatment was most effective when irradiation was administered within 6 to 14 days of the clinical onset of the disease. After 14 days, the successful response rate dropped by approximately 50 percent. The authors' conclusion is that LD-RT offers excellent potential as a treatment for interstitial pneumonia, especially when used during the early stages of the disease [4].

The anti-inflammatory efficacy of LD-RT has been confirmed in several experimental models, both in vitro and in vivo, as well as in different clinical studies. The radiobiological mechanisms that confirm this claim are increasingly known. low doses of RT (0.5-1.5 Gy) act on cells that participate in the inflammatory response, producing anti-inflammatory effects [5].

Evidence from laboratory studies demonstrated the maximum anti-inflammatory effect of RT at doses of 0.3 - 0.7 Gy per fraction. Similarly, in vitro experiments demonstrated that the anti-inflammatory effect of low doses of RT was maximum at 48 h after irradiation and was lost after 72 h. This explains why it is recommended to administer the dose in separate fractions every 48-72 hours.

It seems that there are two different but overlapping pathological subsets, the first triggered by the virus itself and the second, the host response, and which takes place in 3 stages that can be differentiated. In the first stage patients will benefit from drug therapy directed against the virus but not in advanced stages. In the second stage viral multiplication and localized inflammation in the lung is the norm. It is at this stage that most COVID-19 patients would need to be hospitalized for observation and treatment. Patients are likely to require mechanical ventilation and the use of anti-inflammatory therapy may be helpful. A minority of patients will progress to the third and most severe stage of the disease, which manifests as an extra-pulmonary systemic hyperinflammation syndrome.

The use of immunomodulatory agents to reduce systemic inflammation before it leads to multi-organ failure. In this phase, low-dose pulmonary RT could be effective by acting as a potent anti-inflammatory agent against the cascade of pro-inflammatory cytokines.

Recent studies have shown that low doses (≤1 Gy) have anti-inflammatory properties, decreasing the expression of cytokines such as IL-1β and inhibiting the recruitment of leukocytes, thus being able to reduce inflammation and alleviate symptoms that threaten the disease lifetime.

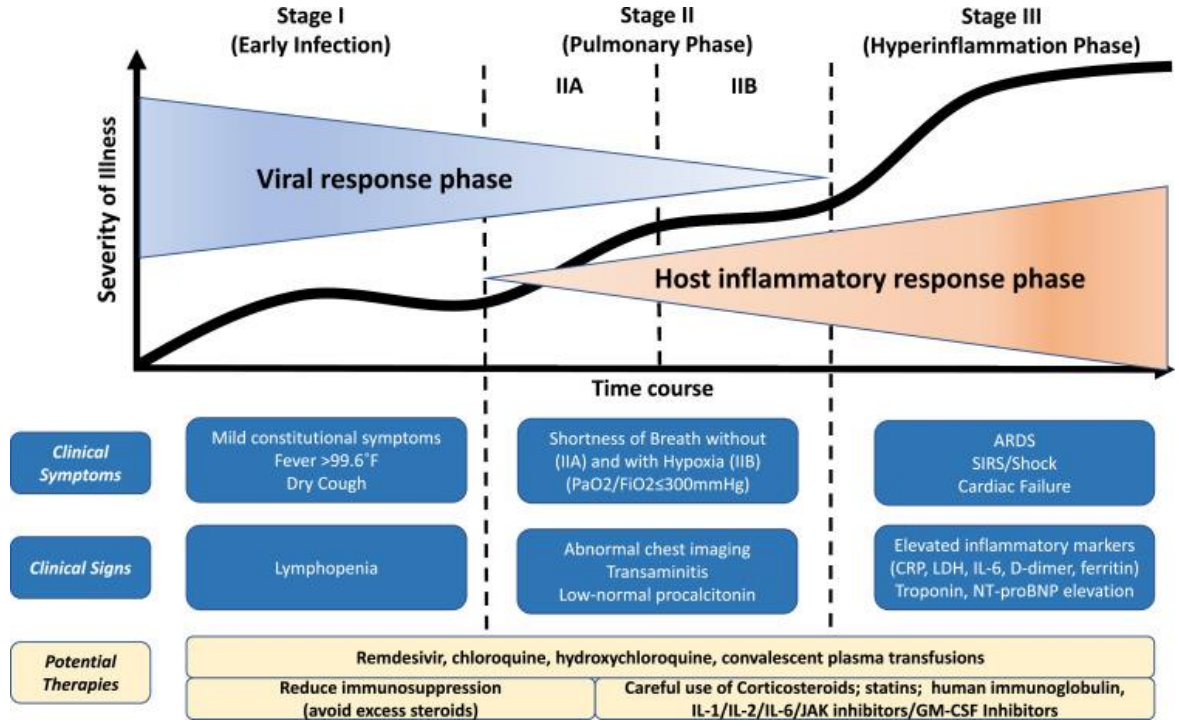

Figure 1 - Classification of COVID-19 disease states and potential therapeutic targets.

The figure 1 illustrates 3 escalating phases of COVID-19 disease progression, with associated signs, symptoms, and potential phase-specific therapies. ARDS, acute respiratory distress syndrome; CRP, C-reactive protein; JAK, janus kinase; LDH, lactate dehydrogenase; NT-proBNP, N-terminal pro B-type natriuretic peptide; SIRS, systemic inflammatory response syndrome; GM-CSF, Granulocyte Macrophage Colony Stimulating Factor.

There are several advantages associated with the use of LD-RT such as that RT treatment units are available, and the proposed treatment procedure is optimized to simplify its development as much as possible. Furthermore, the goal of this treatment is pragmatically designed to be used in a subgroup of patients with limited treatment alternatives and who in the current situation are not candidates for mechanical ventilation and intensive care units.

The doses that have been administered are low (<1% of the doses administered for the treatment of cancer) and do not exceed the tolerance doses of healthy organs, such as the heart. Although the magnitude of the benefit of the proposed treatment is uncertain, it can be affirmed that the probability of harm is very low. For reference, a chest CT scan is about 5 CGy. Therefore, this treatment would amount to the order of 6-10 CTs, well below the known threshold for any typical radiation side effects. What is not clear is whether this low dose could unfavourably modulate the immune environment to exacerbate the underlying lung dysfunction, although the previously cited laboratory and experimental animal studies have not observed this. The safety of low doses of RT has been analysed by different studies that use it for the treatment of benign non-tumour pathology, concluding in all of them that the risk of presenting complications attributable to irradiation is extremely low with the doses suggested in this study. Regarding the induction of secondary malignant tumours, estimates suggest risks of the order of 1 in 1000.

1.2.1. Project Methodology

A simulation CT scan was performed in all patients using a simple, repositionable immobilization device (pillow and leg wedge) for the exclusive use of COVID-19 patients.

The volume of both lungs to which the margin was increased by 5 mm in all directions, except cranio-caudal, which was 10 mm, will be determined as clinical target volume (CTV). The planning was carried out with the objective of achieving a homogeneous distribution in the area to be treated.

The heart was delimited as an organ at risk and the received dose was calculated, although given the ultra-low doses, it was not necessary to establish dose limits in critical organs beyond the ALARA principle (As Low As Reasonably Achievable). Patients receive a dose of 0.5 Gy in a single dose and in case of ineffectiveness at 48 hours, the 0.5 Gy dose should be repeated.

For the preparation and administration of the irradiation, all the necessary measures were followed to guarantee the safety of patients and staff regarding the risk of contagion of SARS-CoV-2, following the regulations and instructions of each center. On the day of treatment, two technicians with the appropriate personal protective equipment position the patient, respecting the protocol available in the Radiation Oncology Service, and will perform the RT planning CT. A third technician is in charge of performing and controlling the examination from the CT console. Later the lungs will be delimited, the doctor defines the PTV and the dosimetric calculation is carried out. While dosimetric calculations are being performed, two technicians, place the patient in the treatment unit. A third technician and the doctor verify the correct positioning (by means of a planar or tomographic image) and the treatment is carried out.

After the treatment, the patient is removed from the unit by the two technicians equipped and returns to her room. Treatment of patients with COVID-19 pneumonia is performed in the same linear accelerator, grouping all patients in a time slot to avoid the risk of contagion to other patients. After the end of the treatments, the treatment room is decontaminated, according to the established protocol. The patient continues to be monitored in the hospitalization unit and control chest CT will be performed on days +7 and +30.

1.3 Objectives

General objectives: Quantitatively and objectively assess changes in chest CT after LD-RT treatment using image recognition and analysis algorithms.

Specific objectives:

- Creation of an image processing algorithm to determine the effectiveness of LD-RT.
- Know the possible advantages and reasons for the use of low-dose radiotherapy for COVID-19 patients.

1.4 Memory Guide

This report is structured as follows: first, the theoretical framework is developed with the explanation of the main parts of the project. Next, we have the section of the materials used in the project. Then we have the methods used for the evaluation of thoracic CT images. Within this section the different algorithms that have been generated are developed. The end of this section corresponds to the algorithm for evaluating the data obtained.

The results section is explained below, dividing this between algorithm results and clinical results. Finally, we have the discussion and conclusions section, obtained during and after the completion of this study, as well as future lines.

2 Theoretical Framework

2.1 Radiotherapy

Radiation therapy is a cancer treatment that uses intense beams of energy to kill cancer cells. LD-RT is used in x-rays to see inside the body, such as teeth or broken bones. RT therapy uses mostly X-rays, although protons or other types of energy may also be used. RT is a local treatment, i.e., it treats the affected area at its source. The long-term goals of RT are to increase local control as well as patient survival.

2.1.1. Anti-Inflammatory Effects of Low Doses Radiotherapy (LD-RT)

Different publications have demonstrated the efficacy of LD-RT in subgroups of patients where the therapeutic benefits of radiotherapy outweigh its potential risks, reserving its use to those cases that do not respond to conventional lines of treatment or to those diseases that, although benign, they are life-threatening and do not have the option of being treated medically. The main biological mechanism involved in the action of LD-RT is the anti-inflammatory effect, which has an analgesic effect. High-dose RT, induces the production of pro-inflammatory cytokines, leading to an inflammatory response in the irradiated tissues. Paradoxically, LD-RT has the ability to modulate an on-going inflammatory response, producing an anti-inflammatory effect.

The efficacy of LD-RT has been demonstrated in the treatment of degenerative bone and inflammatory diseases, such as osteoarthritis, humeral epicondylitis, scapular-humeral periarthritis, or heel spurs. Despite its effectiveness in clinical practice, little is still known about the mechanisms through which LD-RT modulates the various phases of the inflammatory response and about the optimal dose fractionation [6].

2.2 Coronavirus

Coronavirus disease 2019 (COVID-19) is the fifth pandemic after the 1918 flu pandemic. The earliest symptom onset date was December 1, 2019 in the city of Wuhan, China. The symptoms of these patients, including fever, malaise, dry cough, and dyspnea, were diagnosed as viral pneumonia [7]. Initially, the press called the disease Wuhan pneumonia because of the area and symptoms of pneumonia. The results of the whole genome sequencing showed that the causative agent is a new coronavirus [8].

The World Health Organization (WHO) temporarily named the 2019 novel virus novel coronavirus (2019-nCoV) on January 12, 2020 and then officially named this infectious disease coronavirus disease 2019 (COVID-19) on February 12, 2020 Later, the International Committee for the Taxonomy of Viruses (ICTV) officially designated the virus as SARS-CoV-2 based on phylogeny, taxonomy, and established practice. Since COVID-19 initially emerged in China, the virus has evolved and rapidly spread to other countries around the world as a global threat. On March 11, 2020, the WHO finally made the assessment that COVID-19 can be characterized as a pandemic, after the 1918 Spanish flu (H1N1), the 1957 Asian flu (H2N2), the Hong Kong flu. 1968 (H3N2) and 2009 (H1N1) pandemic flu [9].

In order to understand the severity of this global pandemic, the figure 2 shows a graphic representation of the new daily deaths confirmed by COVID-19 around the world. We can see in the graph that despite the fact that it is an oscillating value since the start of the pandemic this has been a constantly increasing value. This number has not been able to descend to a minimum value that allows guaranteeing the health security of the population [10].

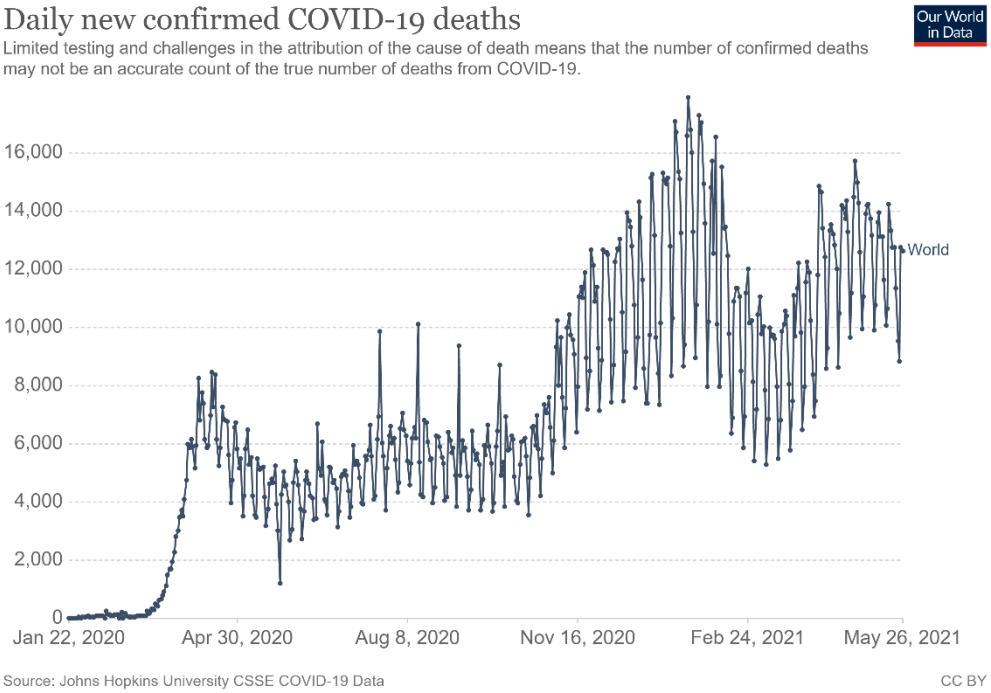

Figure 2 - New Daily Global Confirmed COVID-19 Deaths

2.3 Computed Tomography (CT)

The term "computed tomography" (CT), also called computerized axial tomography, is a computerized x-ray imaging procedure in which a narrow beam of x-rays is directed at a patient and rotates rapidly around the body, producing signals that they are processed by the machine's computer to generate cross-sectional images ("slices"), displayed in figure 3. These slices are called tomographic images and contain more detailed information than conventional X-rays. Once the machine's computer obtains several successive slices, they can be "stacked" digitally to form a 3D image of the patient, thus detecting abnormalities in the patient's structure [11].

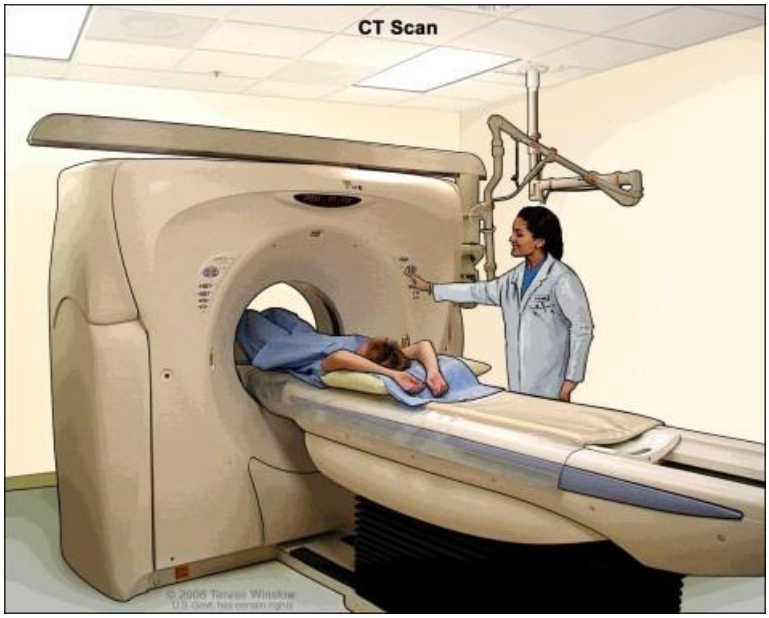

Figure 3 – Drawing of the patient on a table that slides through the CT machine

Unlike a conventional X-ray, which uses a fixed X-ray tube, a CT scanner uses a motorized X-ray source that rotates around a circular opening in a structure like the one seen in the image and receives Gantry's name [11].

During a CT scan, the patient lies on a bed that moves slowly through the gantry, while the X-ray tube rotates around the patient, shooting narrow beams of x-rays through the body. Instead of film, CT scanners use special digital x-ray detectors, which are located directly opposite the x-ray source. As the x-rays leave the patient, they are picked up by the detectors and transmitted to a computer. Each time the x-ray source completes one full rotation, the CT computer uses sophisticated mathematical techniques to construct a 2D image slice of the patient. The thickness of the tissue represented in each image slice can vary depending on the CT machine used, but usually ranges from 1-10 millimetres. The process continues until a certain number of sections is obtained, thus obtaining a 3D image of the desired area of the body. This method has many advantages, including the ability to rotate the 3D image in space or view slices in succession, making it easy to find the exact place where a problem might be located [11].

It is easy to image dense structures in the body, such as bone, while soft tissues vary in their ability to stop x-rays and are therefore difficult to visualize. This is the reason why contrast media are used, which contain substances that better stop X-rays, allowing higher quality images to be obtained [11].

When it comes to the safety of CT scan, there are very few risks associated with it. However, the risk of developing cancer may be increased if numerous examinations are performed with this technique, since there is a higher exposure to ionizing radiation than in conventional radiography. For this reason, it is important that CT scans are limited to only those cases where the benefit that can be obtained significantly outweighs the increased risk. This is the reason why special care must be taken in children, since they are more sensitive to ionizing radiation and have a longer life expectancy, therefore, they have a relatively higher risk of developing cancer than adults. Also, the smallest size of a child affects the amount of radiation dose received. For these reasons, the equipment settings must be adjusted, and the radiation dose reduced when performing CT on a child [11].

Depending on the specific characteristics of each patient, allergic reactions (pruritus, itching), even kidney failure due to the use of contrast media may also occur. CT is not recommended in pregnant women, since it could cause congenital malformations; in this case, ultrasound and / or magnetic resonance imaging would be used [12].

The first CT apparatus that worked effectively and had clinical application was carried out by Hounsfield in 1967. The technique has evolved over the years, and today helical computed tomography is used, by means of which images are taken continuous in the form of a spiral, instead of individual images as at the beginning. Some of the advantages of helical computed tomography, compared to older CT techniques, is that it is faster, allows better 3D images of internal body regions, and can detect small abnormalities with better precision. The most recent CT scanners are the so-called multidetector CT scanners, which allow more images to be obtained in a shorter time. This type of technique plays a fundamental role in the follow-up of colorectal cancer operated patients, since it makes it possible to recognize complications and recurrence [13].

2.3.1. Chest CT

Chest CT scan uses special x-ray equipment to examine abnormalities found on other imaging tests, and to help diagnose the cause of an unexplained cough, shortness of breath, chest pain, fever, and other chest symptoms [14].

2.4 Medical imaging

Medical imaging is an indispensable component of modern medical science and practice. It is uncommon to diagnose or treat a medical condition without taking advantage of medical imaging because of the incredible level of anatomical and functional details that the medical images reveal about the human body. Medical imaging has created a virtual window into the body, fostering a better scientific comprehension of its mysteries, enabling the investigation of underlying causes of medical symptoms through diagnostic processes, and aiding in disease treatment through proper targeting and monitoring [15].

One key advantage of medical imaging lies in its foundational format. As the body is an incredibly complex system, one of the major challenges for both research and clinical care is the comprehension of its vast quantities of information in such a way that it can be assimilated, interpreted, and utilized. Imaging provides a significant depth of quantitative information that can be deciphered through computational analyses [15].

2.4.1. Historical Foundation

To appreciate the role of imaging in modern medicine, it is helpful to consider the historical context and the importance of physics principles. In the 1800s and before, physicians were extremely limited in their ability to obtain information about the illnesses and injuries of patients. They relied essentially on the five senses, and what they could not see, hear, feel, smell, or taste usually went undetected. Even these senses could not be exploited fully because patient modesty and the need to control infectious diseases often prevented full examination of the patient. Frequently, physicians served more to reassure the patient and comfort the family rather than to intercede in the progression of illness or facilitate recovery from injury [16].

The twentieth century has witnessed remarkable changes in the physician's ability to intervene actively on behalf of the patient. These changes have dramatically improved the health of humankind around the world. In developed countries, infant mortality has decreased substantially, and the average life span has increased. Many major diseases have been brought under control, and some have been virtually eliminated. Diagnostic medicine has become commonplace, and therapies have evolved for cure or maintenance of persons with a variety of maladies [16].

In this progress of modern medicine, medical imaging has been a significant contributor by offering diagnostic probes to identify and characterize problems in the internal anatomy and physiology of patients. Medical imaging has been instrumental in moving the physician into the role of an active intervener in disease and injury and has a major influence on the prognosis for recovery [16].

In November 1895, Wilhelm Röntgen, a physicist at the University of Würzburg, was experimenting with cathode rays. He discovered that radiation (X-rays) could penetrate various materials and be etched on photographic plates.

Over the first half of the twentieth century, X-ray imaging advanced with the help of improvements such as intensifying screens, hot-cathode X-ray tubes, rotating anodes, image intensifiers, and contrast agents.

Through the 1950s and 1960s, diagnostic imaging progressed as a symbiosis of X-ray imaging with the emerging specialties of nuclear medicine and ultrasonography. The application of physics to medicine in the 1900s established the foundation for modern medical imaging and enabled the progress observed to date. In the current practice of medical imaging, close concordance with radiologic physics is the foundation of precision and innovation of the operation [16].

2.4.2. Medical imaging processing

Medical image processing encompasses the use and exploration of 3D image datasets of the human body, obtained most commonly from a CT or Magnetic Resonance Imaging (MRI) scanner to diagnose pathologies, or guide medical interventions such as surgical planning, or for research purposes. Medical image processing is carried out by radiologists, engineers, and clinicians to better understand the anatomy of either individual patients or population groups.

The ever-improving quality of imaging coupled with advanced software tools facilitates accurate digital reproduction of anatomical structures at various scales, as well as with largely varying properties including bone and soft tissues. Measurement, statistical analysis, and creation of simulation models which incorporate real anatomical geometries provide the opportunity for more complete understanding, for example of interactions between patient anatomy and medical devices.

The process of medical image processing begins by acquiring raw data from CT or MRI images and reconstructing them into a format suitable for use in relevant software. A 3D bitmap of greyscale intensities containing a voxel (3D pixels) grid creates the typical input for image processing. CT scan greyscale intensity depends on X-ray absorption, while in MRI it is determined by the strength of signals from proton particles during relaxation and after application of very strong magnetic fields.

For medical users, the reconstructed image volume is typically processed to segment out and edit different regions of anatomical interest, such as tissue and bone.

2.4.3. Key problemes

In order to understand the extensive role of imaging in the therapeutic process, and to appreciate the current usage of images before, during, and after treatment, we focus our analysis on four main components of image-guided therapy and image-guided surgery: localization, targeting, monitoring, and control [17].

Specifically, in medical imaging we have four key problems:

1) Segmentation: automated methods that create patient-specific models of relevant anatomy from images
2) Registration: automated methods that align multiple data sets with each other
3) Visualization: the technological environment in which procedures can be displayed
4) Simulation: software that can be used to rehearse and plan procedures, evaluate access strategies, and simulate planned treatments.

3 Materials

3.1 Software

First of all, and before we start with the processing of the DICOM images, we are going to view them by computer. The software used for this is MicroDicom. MicroDicom is application for primary processing and preservation of medical images in DICOM format. It is equipped with most common tools for manipulation of DICOM and it has an intuitive user interface.

As far as image processing is concerned, within the wide variety of existing programs we will use Matlab software. MATLAB (short for MATrix LABoratory, "matrix laboratory") is mathematical software that offers an integrated development environment (IDE) with its own programming language (M language). This software, one of the most used in engineering, is a powerful mathematical tool. Additionally, you can extend MATLAB's capabilities with toolboxes. In the case of image manipulation, the "Image Processing" toolbox is used [18].

3.2 Files

3.1.1. DICOM

DICOM (Digital Imaging and Communications in Medicine) is a standard developed in 1983 by the American College of Radiology (ACR) and the National Electrical Manufacturers Association (NEMA). They formed a committee whose mission was to find or develop an interface between the equipment and any other device that the user wishes to connect. In addition to the specifications for the hardware connection, the standard was developed to include a dictionary of the data elements necessary for image interpretation and display [19].

The standard describes the file format and specification of a patient's primary data in the image, as well as the required header, describing a language common to different medical systems. In this way, the images are accompanied by measurements, calculations, and descriptive information relevant to diagnoses. Use files with a .dcm extension

A single DICOM file contains a header that stores information about the patient's name, scan type, image dimensions, etc. as well as a special attribute that contains the pixel data for the image. A single DICOM object can only have one attribute that contains pixel data. For many modalities, this corresponds to a single image. However, the attribute can contain multiple "frames", allowing the storage of cine loops or other multi-frame data. In these cases, the 3D or four-dimensional data can be encapsulated in a single DICOM object [19].

The main application of the DICOM standard is to capture, store and distribute medical images. DICOM information object definitions encode data produced by a wide variety of imaging device types, including MRI, CT, positron emission tomography, endoscopy, microscopy, and more. DICOM is also used with devices associated with imaging or imaging workflow, including image viewers, and viewing stations, 3D display systems, clinical analysis applications, image printers. It is for all this that it is one of the most used standards for image storage in the medical sector [19].

According to a paper presented at an international symposium in 2008, the DICOM standard has problems related to data entry. "A big disadvantage of the DICOM standard is the possibility of entering probably too many optional fields. This disadvantage is mainly shown in the inconsistency of filling all the fields with the data. Some image objects are often incomplete because some fields are left blank and others full of incorrect data". This in our case is not a problem for image processing so we will not take it into account [20].

3.1.2. Data

The images used for this TFG correspond to the study "*RADIOTERAPIA ANTI-INFLAMATORIA A DOSIS BAJAS PARA EL TRATAMIENTO DE LA NEUMONÍA POR COVID-19: ESTUDIO PROSPECTIVO MULTICÉNTRICO (IPACOVID)"* carried out by the radiotherapy oncology unit of the Sant Joan University Hospital, Reus. These are chest CT images of 31 patients stored in DICOM format, section by slice, that is, each slice of said CT corresponds to a single DICOM file. The patients have been both men and women between 69 and 94 years of age. Specifically of the 31 patients, 17 were men and the remaining 14 were women. Table 1 shows the clinical characteristics od the patients.

The images of the patients are helical sections all taken following the same protocol, maintaining the same parameters and the same tomography apparatus. They are obtained in gray levels according to the specific characteristics of ISO_IR 100. The size of the volumes differs depending on each patient, in addition the dimensions of the matrices vary.

In addition, an excel file has been used where clinical information about the patients is stored. In the table below we have a list with the characteristics of these patients as well as the average values or the percentages of each of them.

Variables		(n = 30)
Age		84.8 (69-94)†
Sex		
	Female	14 (46.6)‡
	Male	16 (53.3)‡
Neurologic diseases		8 (26.6)‡
Cardiovascular diseases		24 (80)‡
Respiratory diseases		11 (36.6)‡
Other comorbidities		24 (80)‡
Days with symptoms		5.1 (2 - 7)†
Functional status (Barthel Index)		
	Independent	8 (26.6)‡
	Minimally dependent	1 (36.6)‡
	Partially dependent	5 (16.6)‡
	Very dependent	4 (13.3)‡
	Very severe dependent	-
Geriatric Depression Scale (GDS)		
	No cognitive decline	17 (56.6)‡
	Very mild cognitive decline	6 (20)‡
	Mild cognitive decline	5 (16.6)‡
	Moderate cognitive decline	-
	Moderately severe cognitive decline	2 (6.6)‡
	Severe cognitive decline	-
	Very severe cognitive decline	-
Pharmacological treatment		
	Corticoisteroids (dexamethasone)	36 (100)‡
Basal SpO2		94.28 (89 - 96)†
Basal *SaFi		255.42 (89 - 462)†
	Mild	15 (50)‡
	Moderate	5 (16.6)‡
	Severe	10 (33.3)‡
Basal *PaFi		251.39 (128.19)‡
	Mild	22 (73.3)‡
	Moderate	3 (10)‡
	Severe	5 (16.6)‡
*CURB-65 Score		
	1 point	-
	2 points	10 (27.8)‡
	3 points	17 (47.2)‡
	4 points	9 (25)‡
*CT lung involvement (%)		
	<5%	-
	5-25%	1 (3.3)‡
	26-50%	6 (20)‡
	51-75%	15 (50)‡
	>75%	8 (26.6)‡
Final status		
	Alive	23 (76.6)‡
	Exitus due to covid-19	8 (26.6)‡
	Exitus other causes	5 (16.6)‡

Table 1 - Clinical characteristics of patients with COVID-19 treated with low-dose radiation therapy.

**CT (Computed Tomography); CURB-65 (*CURB-65: validated clinical prediction score for predicting mortality in community-acquired pneumonia and infection of any site including measurement of: Confusion of new onset, Blood Urea Nitrogen, Respiratory rate, Blood pressure and Age*); PaFi (ratio of arterial oxygen partial pressure (PaO2) to Fractional Inspired Oxygen (FiO2)); SpO2 (oxygen saturation); SaFi (ratio of SpO2 to FiO2).*

†Results shown as means and range in parenthesis.

‡ Results shown as means and percentages in parenthesis.

4. Methods

4.1. Collection of images

The images have been stored in their corresponding order. For the use of this study, the patients will be named by their identification number, (included in these files), thus trying not to reveal personal information of the patients and that they remain anonymous.

The images were stored in individual folders for each patient whose title was the patient's identification number. Within each of these folders we have 3 other folders with the titles, Basal, Week and Month. These names refer to the period during the treatment in which the CT was performed and within each one are the corresponding DICOM files.

4.2. Modification and Classification

4.2.1. Modification

As we have commented previously, each of our DICOM files corresponds to a CT section, that is, a 2D image. Although we could carry out the image processing from these files, it is much easier to work with 3D files, that is, a single DICOM file contains the entire CT. We decided to work with the 3D files instead of the 2D files since our main evaluation is based on the calculation of the lung volume and for this, we need the files in 3 dimensions.

As our images are in 2D to be able to convert them to 3D we will use the MicroDicom software. In order to open our individual files as a single file in this program, we need all the sections of the same CT to be in the same folder compressed in .zip.

Once we have this from the MicroDicom interface we can open this folder and we will see that all our files are arranged in an orderly way in the viewer. Next, we have to export our files in DICOM format but selecting the option "export current series", displayed in figure 4. With this we will create the file.

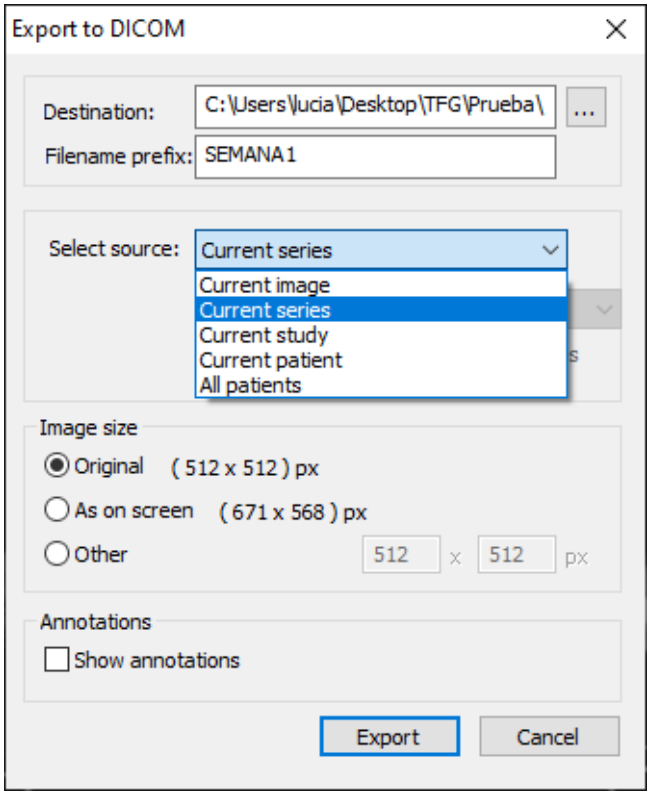

Figure 4 - DICOM file export screen as 3D files all in the same series

We will save each file with its name corresponding to the period in which the CT scan was performed, these being Basal for the CT scan performed on the first day, Week, for the CT scan that was performed a week after having performed the radiotherapy treatment and Month for the CT scan that was performed one month after the radiotherapy treatment was performed.

4.2.2. Classification

A fundamental part of this project is the previous classification of the files. In order to be able to process them properly, a classification similar to that carried out during the collection of the files has been chosen. Each patient has their own folder with their identification number and within this three DICOM files corresponding to the three CTs that have been made, as seen in the figure 5.

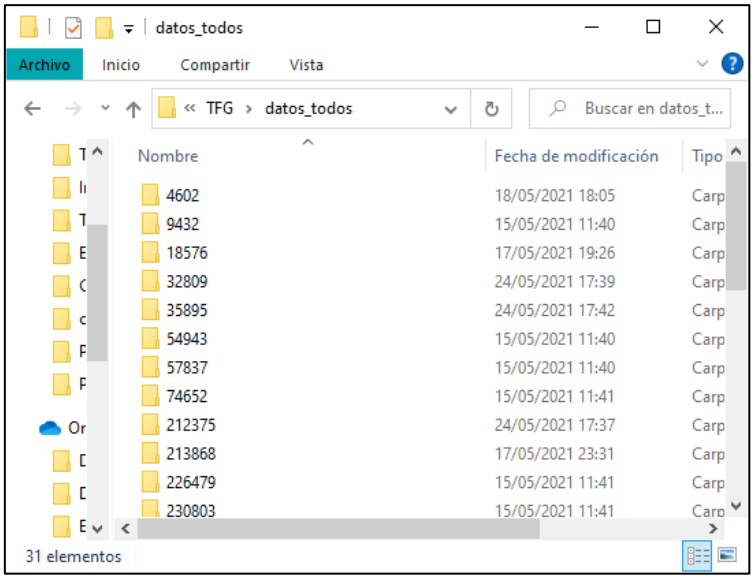

Figure 5 - General directory with the division of folders for each patient identified with their ID number

Each corresponds to a CT scan performed to the patient in the corresponding period being "basal" the first CT, before receiving radiation therapy, "week" CT performed one week after receiving radiation therapy and "month" CT performed one month after receiving radiation therapy. Displayed in figure 6.

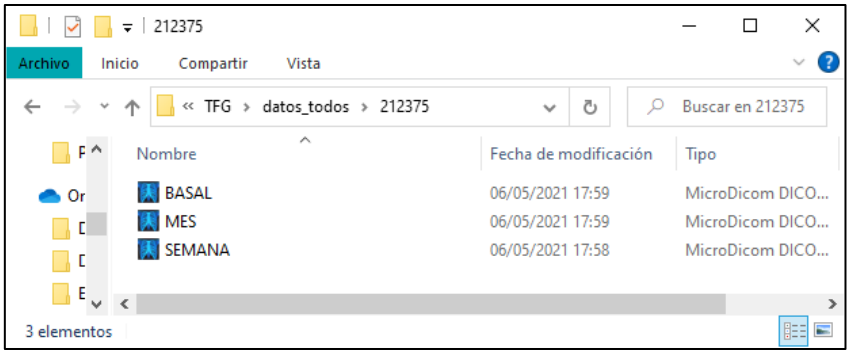

Figure 6 - Folder of a patient with its three DICOM files inside. Each one corresponding to the TACs that have been carried out

4.3. Image Processing Algorithms

The main goal of image processing is to calculate the lung volume of the three CT scans for each patient. As mentioned before, we will use DICOM files. These files can be treated as 3D images or as 2D images. In order to achieve a more accurate volume measurement, two different algorithms have been created, one of them evaluating 2D images and the other evaluating 3D structures. As we will see later, the 2D algorithm is the one with which the best results have been obtained, so it will be the main algorithm that we will describe. We will also describe the 3D algorithm in brief.

In both, 4 different functions have been implemented, these being "main", "principal", "lung" and "mask" as well as a script to carry out the evaluations.

4.3.1. 2D Volume calculation algorithm enhanced with information of the previous CT section

This is the main algorithm that has been used for the evaluation of patient lung volumes. It is called a 2D algorithm since it analyzes the sections as 2D images to evaluate the lung area. Calculating the lung areas of all the sections where there are lungs and adding later the lung volume is obtained.

Although we call the algorithm "2D" it does not evaluate the images separately, but rather it evaluates the images as consecutive sections to make comparisons between them. This is done by creating two-dimensional masks of each section and comparing these masks with the one generated in the previous section. Thus, it is possible to stop the algorithm for evaluating pulmonary areas just in those sections in which there is no lung.

Next, we will explain the code of each of the functions. We will explain these functions "from the outside in", that is, from the outermost code to the innermost code. We will start with the "main" function. A detailed explanation with step-by-step photos of this algorithm has been included in the annex.

4.3.1.1. Main

This function corresponds to the beginning of the code. First, we have three commands: clc (clear command window) to clear all text from the command window, resulting in a clean screen, close everything that closes all figures whose handles are visible, and clear everything that clears all variables of the current workspace. Then we use the dir command to read the directory in which our patient folders are located, and we save it in the variable num_dir. This variable is of type structure. Next, we call the main_function function to which we introduce the variable num_dir by parameter. We save the data obtained in the data variable.

To save the data obtained, what we will do is load an excel file. This file is an excel file provided by the Sant Joan Hospital, it is a compilation of the data of the patients included in the project. We will join the table obtained with the table from excel with the join function. Then we will use the writetable command to create an excel and save our new table. This table contains all the data necessary to evaluate the results. This evaluation will be done in a different script.

4.3.1.2. Principal

Now we have the second function, called *"PRINCIPAL"* function*.* This function is used to evaluate all patients and read the three DICOM files for each patient. Then these data are passed to the *"LUNG"* function to calculate the lung volume and this data is stored in a table called *datas*. See figure 7.

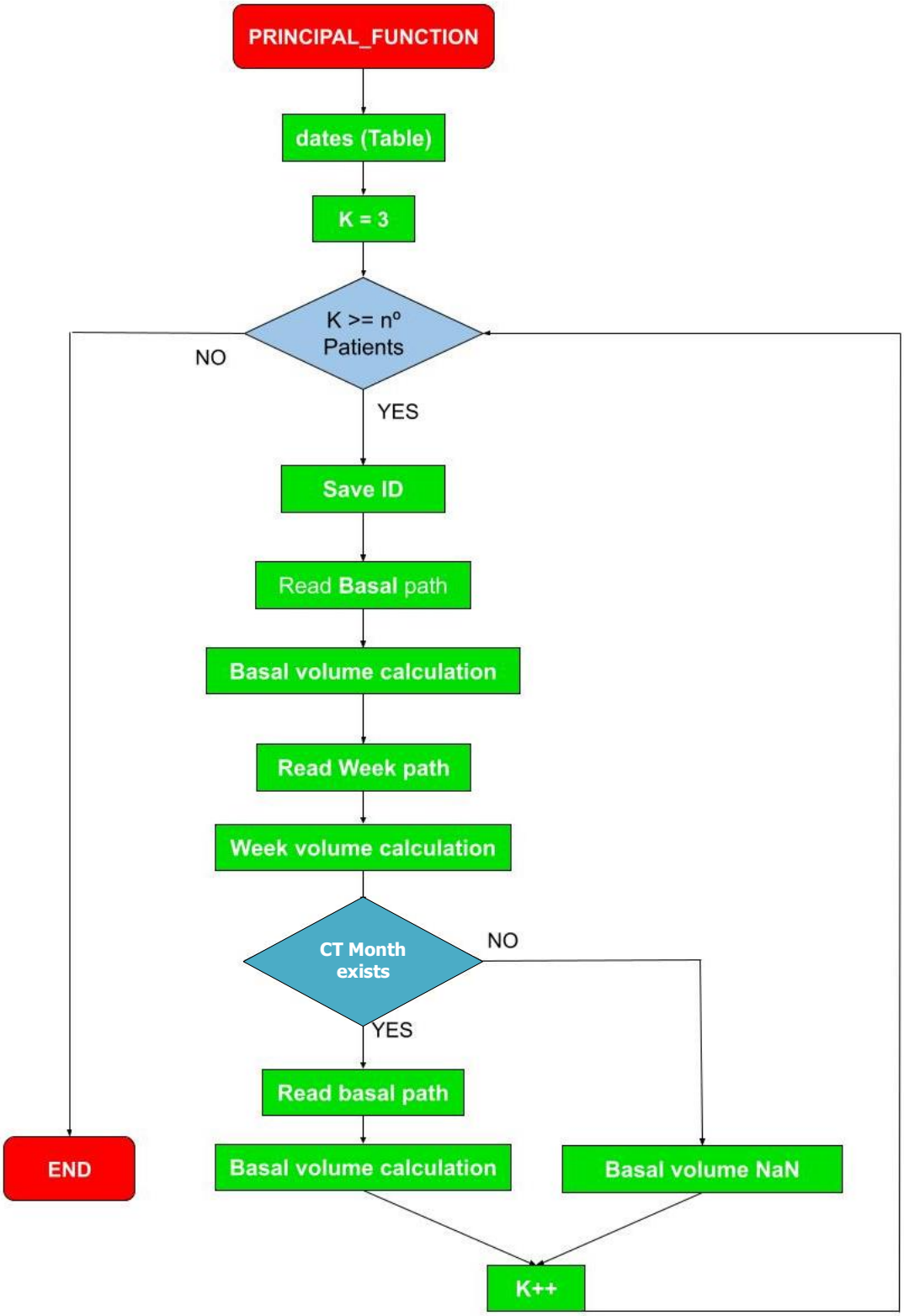

Figure 7 - Principal function flow chart

The first thing we are going to define are the inputs and outputs of the function. This function receives as input a variable called *num_dir* that is of type struct, which has several types of variable, but we will focus on the variable called "*name*". This variable contains the names of the folders in which the CTs of our patients are located, that is, their identification number (ID).

The first thing is to define the data variable, which is the table where we will store the information about lung volumes as well as the ID of each patient. This table has a dimension equal to the number of folders we have in our directory, that is, the length (num_dir) multiplied by 4. We have to subtract 2 units from this length. This is because the first two values of our variable num_dir are not valid since the dir command, which we will see later, with which this variable has been created takes all the folders in our directory. In all the folders on our computer, in addition to the folders we store, two additional folders are stored, one that refers to the directory's own folder and another that refers to the previous folder. This happens by default in all folders on the computer and they are always read as the first two.

To create this table, in addition to specifying the size, we also have to specify the type of variables that we want to introduce in each column and the name of the columns. It is not necessary to define the name but if we do it later it will be easier for us to access them. We define the types of the variables as 'string' for the first column and 'double' for the other three, since in the first column we will save the "name" of our patient and in the other three the value of lung volumes. We call our patient's identification number "name."

Next, we start the "for" loop that will go through the folders one by one with K as the counter. This counter goes from 3 to the length of our variable num_dir for the reasons explained before.

The first thing we do when starting this loop is to save the identifier of our patient, that is, the name of the folder in the name field of our data variable. We do this using the convertCharsToStrings command to be able to transform the variable num_dir (k) .name which is of type char into string since the cell data.Name (k-2) is of type char.

Throughout the cycle, when we want to store something in any of the cells of the data variable, we will use k-2, that is, the cycle counter minus two. This is because, from what we have explained above, the main counter of the loop is ahead by two units, so if we want to use this counter for the data variable, we must subtract two units from it.

So, we have three almost equal blocks. These three blocks perform the same function, calculating lung volume but each with data from a different CT. The first thing we do is extract the full name of the path in the path_in variable with the strcat command. This command is used to concatenate strings horizontally, so we put as an argument our general directory, the name of the folder that we are exploring and the name of the DICOM file that we want to evaluate. In these three blocks we use three different names of DICOM files, Basal, Week and Month since they are the three CT that we want to evaluate.

Next, we calculate the volume of the lungs. We do this by calling the lung_funcion function, to which we enter the variable path_in, our complete directory, as a parameter. We save the results in the corresponding cell of the data variable. Within the Month block we have a difference since we need an if conditional in case this CT does not exist. This is because there are patients who die before finishing all the treatment. Patients who died before the week's CT could be performed were not considered in the study, so an exception is not necessary in this case. We will check with this *if*, if the CT of the month exists, if so, we will call the *LUNG_FUNCTION* function, but on the contrary, if not, we will assign a *NaN* value ("not a number") to this field.

Finally, this function will return the data variable, which contains the information about the lung volumes as well as the identifier of each patient.

4.3.1.3. Lung

Now we will go on to explain the lung_funcion function. This function is the one that analyzes and processes the CTs one by one. To this function we put the path_in parameter, that is, the directory of our DICOM file and it returns the volume of the lungs by parameter in the variable Vol. See figure 8.

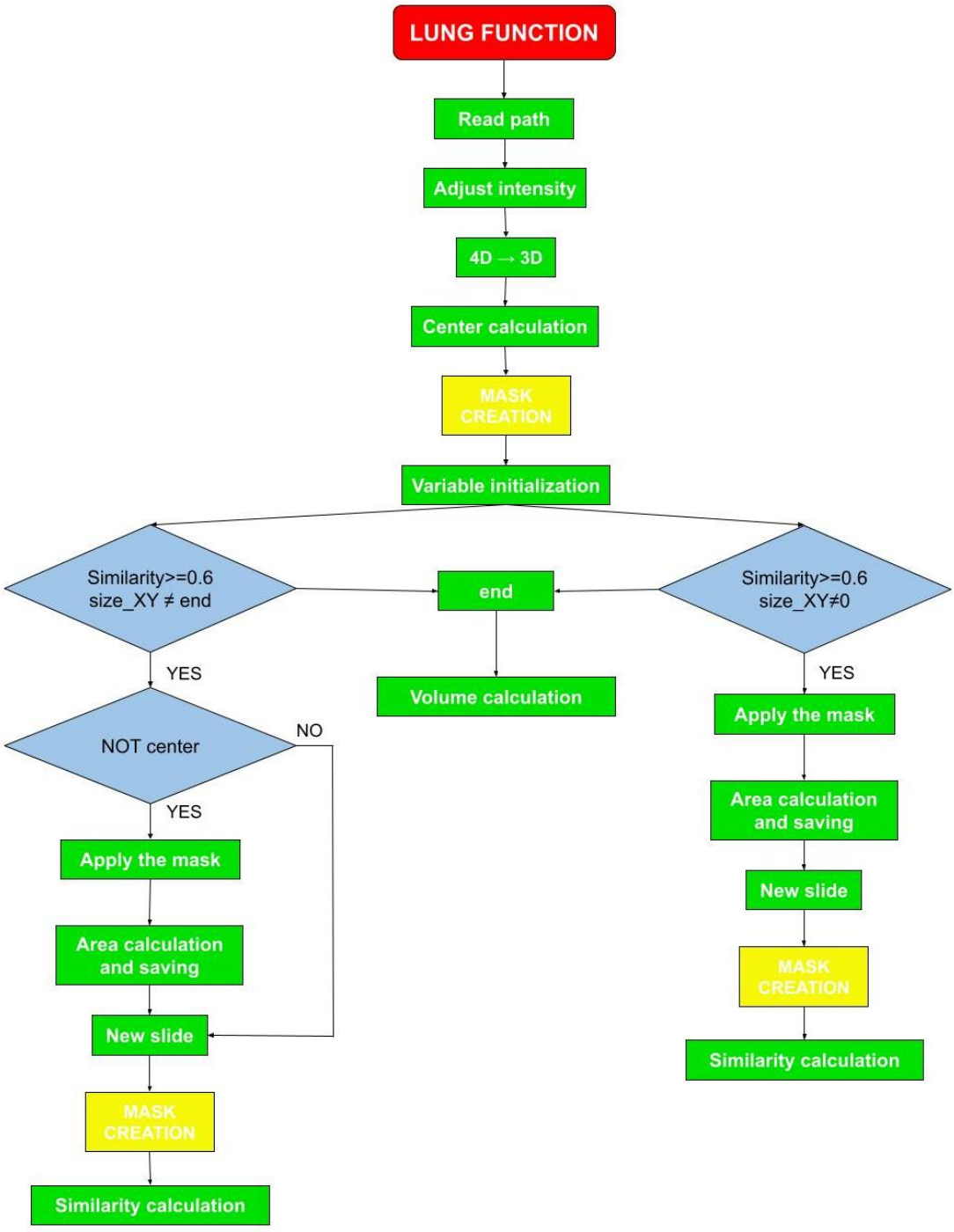

Figure 8 - Lung function flow chart

The first thing we do is read the DICOM file from the directory with the dicomread command and save it in the info variable. Then, we use the im2single method, which converts the intensity image I to single, rescaling the data if necessary and with the imadjustn method we adjust the intensity values of the image. By default, saturates the bottom 1% and top 1% of all pixel values. This operation increases the contrast of the output image.

DICOM images are 4D images but for CT evaluation we will use only 3D. For this reason, the last step before starting to segment the lungs is to go from our 4D image to a 3D image. To do this we assign the value 1 to the third dimension of our 4D image and then we use the squeeze command to eliminate this dimension since this command eliminates those dimensions that are equal to 1. Once we have our file in 3D, we can use the command volumeViewer to display our structure in the workspace, shown in Figure 9.

Before starting to segment the lungs, we will load the excel Values in the workspace. In this table we have two values that will be important in our algorithm, the Value_Similarity that is the similarity value that we will put as a condition and the Value_Threshold that will be the threshold value that we will apply to obtain our masks.

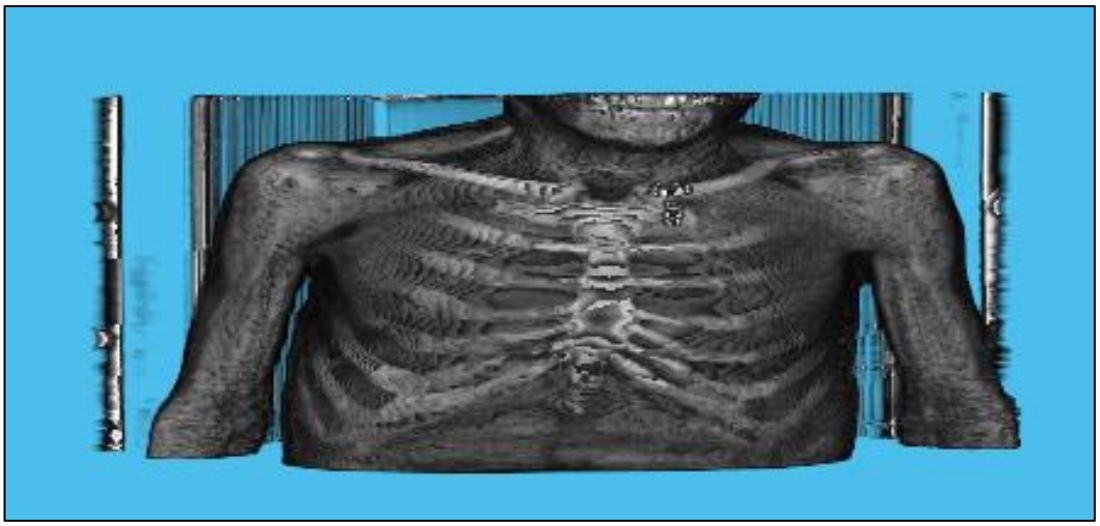

Figure 9 - Representation of the original 3D structure

We now proceed to segment the lungs on the computed tomography data using the active contour technique. Active Contours is a region growth algorithm that requires initial seed points. The Image Segmenter application is used to create this seed mask by segmenting a two-dimensional orthogonal slice in the XY plane. We will apply this process twice since we will start with a section in the middle of the lungs, and we will process up and down to obtain the total lung volume.

The extraction of these sections, the creation and application of these masks as well as the calculation of the lung area will be done section by section. This means that we will process each CT section as an individual image, for this reason we will calculate areas, instead of volumes, to finally add them and thus obtain the total volume.

The first thing is to extract the center section in the XY dimensions, displayed in figure 10. To do this, we extract the dimensions of our image and obtain half of this dimension. The int16 () function is used because we need integer values since this value will act as an index. Once we have this value, we can extract the section. The image obtained can be seen in the following figure.

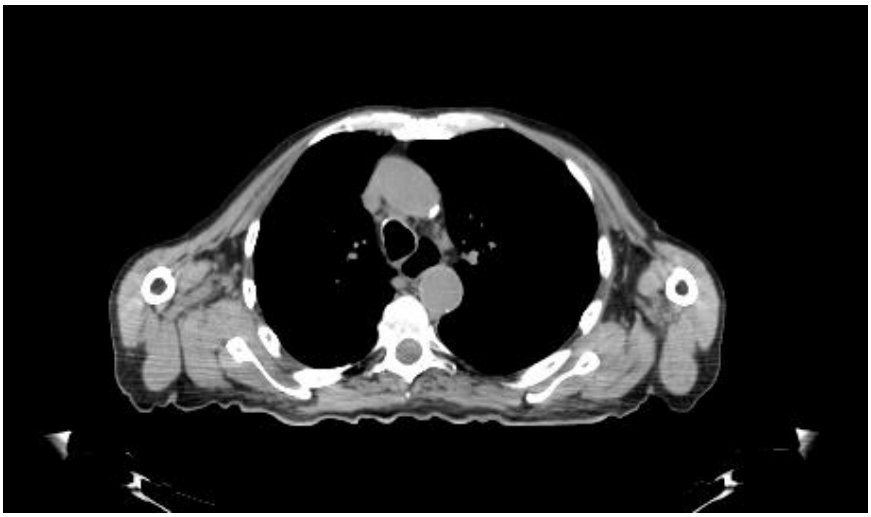

Figure 10 - Central slide of our structure

Once we have extracted the first section, its mask is created. This is done through the MASK function which will be explained later. The application of this mask will be done inside the loops. These are two while loops that depend on two conditions. Before starting these loops we have to define two variables, AreaPixels, which is defined as a double but it will be an array where we will store the values of our areas and the area of the variable, which we will use as a condition in the while loops so we start it with three rows to be able to start the cycle. We also initialize the similarity variable to 1.

We will now analyze the two while loops. Both loops are very similar. In the first loop. in which we will evaluate the upper part of the CT, we have the condition that the area array has at least two dimensions and that we have not reached the end of the CT. While in the second loop we have as a condition that the area array has at least two dimensions and that we have not reached the end of the CT but towards the other end. Before starting this second loop, in addition to resetting the area variable, we have to reset the size_XY variable since it has been modified in the previous loop.

As we have commented, the structure of these loops is very similar. The first thing is to apply the mask corresponding to the section to be treated. At the start of the first loop, the initial mask calculated above is applied to the center section. Our image with the mask applied is shown in the following figure. The rest of the times this loop is executed as well as the second loop, the mask calculated in the previous interaction is applied to the corresponding section. See figure 11.

Figure 11 - Mask for the central slide

The next step is segmentation. To get a quality segmentation, we use histeq to distribute the voxel values in the available range.

Now we perform the calculation of the volume of the segmented lungs. We use the regionprops function with the *'area'* option to calculate the area of the lungs. Area will then be a structure with the values of the areas of our image once we have applied the mask.

As images can have noise, we will order this structure to retain only the two largest volumes, which correspond to our two lungs. To order the structure we have to pass it to table format, we sort it in descending order and return it to structure.

The next section of our 3D image is selected. The corresponding mask for this section is created and this mask is compared with the mask of the previous section. This is done through the command says that it returns a similarity index with values from 0 to 1 with 1 being two identical images. With this we finish the first loop. Once the similarity is calculated if they compare the two initial conditions of the loop again. For our example this would be the mask obtained for the next section. See figure 12

Figure 12 - Mask for the next slide to the center

In the figure 13 we can see the two overlapping masks. The magenta and green parts are those parts that are different in the images. You can also see in the following figure the regions of difference that there are. Between these two masks, a similarity index of 0.9726 has been obtained.

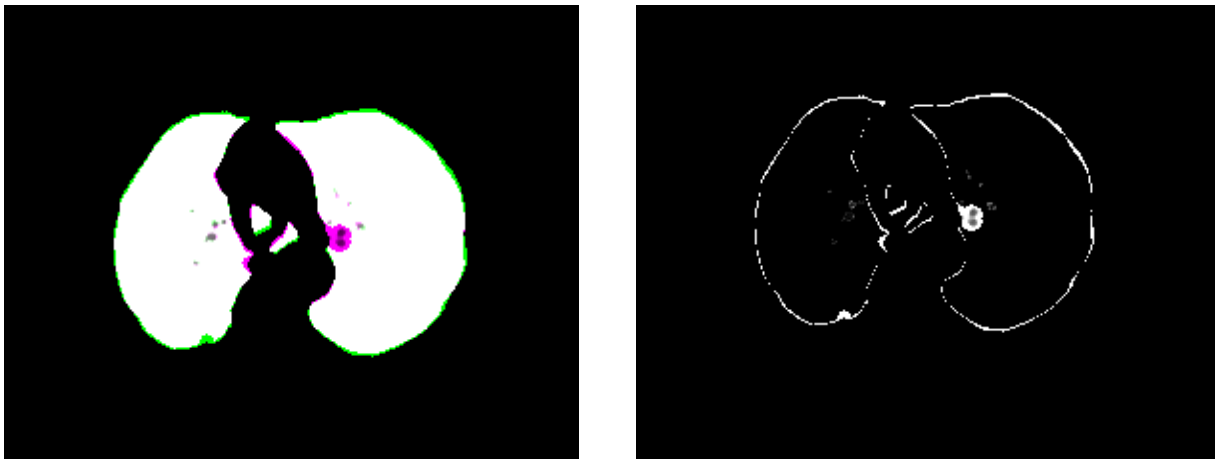

Figure 13 - Differences between the two masks previously calculated.

The two overlapping masks are shown on the left, highlighting the differences colours. On the right, the subtraction of both images is shown, that is, the areas that do not coincide

Before starting the next loop, we have to restore some of our variables again. This second loop is very similar to the previous one except for two differences. First of all, before applying the mask as in the first part of the previous loop, check that the treated section is not the central one. This is done to avoid treating this section twice as it has already been treated in the previous loop. Secondly, the other difference is that in this case the counter increases by 1 unit instead of decreasing by one unit as in the previous loop.

Once these two loops are finished, we will save our total volume. We will first check that the *areapixels* vector is not empty and then we will make the sum of all its values, thus obtaining the lung volume. If the vector *areapixels* is empty, we will assign the value *NaN* to the variable Vol.

To make the evaluations and comparisons of lung volumes we have two options: to compare the data in voxels or in cubic liters. To simplify the procedures and thus avoid calibration errors, the values in voxels will be used. If we wanted to analyze these values in liters we would have to specify the voxel spacing in the x, y, z dimensions that can be collected from the metadata of the original files. As there are no verifications of the accuracy of the calibrations of the tomographs used for the process, we will avoid this step by reducing the calibration error.

4.3.1.4. Mask

The Mask function is very simple and is used to create the mask that we will apply to our image. We can see in the following image the flow diagram of our function. See figure 14.

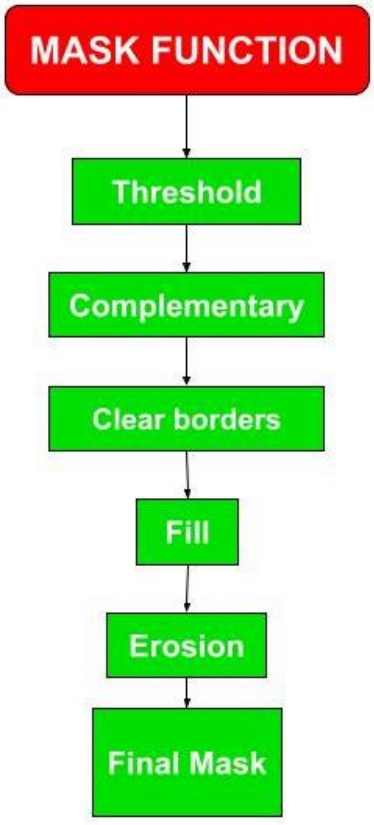

Figure 14 - Mask function flow chart

To create the mask in the XY section by code we will apply a threshold value. This value corresponds to the threshold value that we have entered by parameter and which has been obtained from an excel with our desired values. With this we will have created our mask, which we can see in the figure 15.

Figure 15 - Central slide with threshold valeu applied

With this we will have created our mask but now we will have to adjust and refine it. We will start by inverting the mask with the mismatch so that the lungs are in the foreground. Displayed in figure 16.

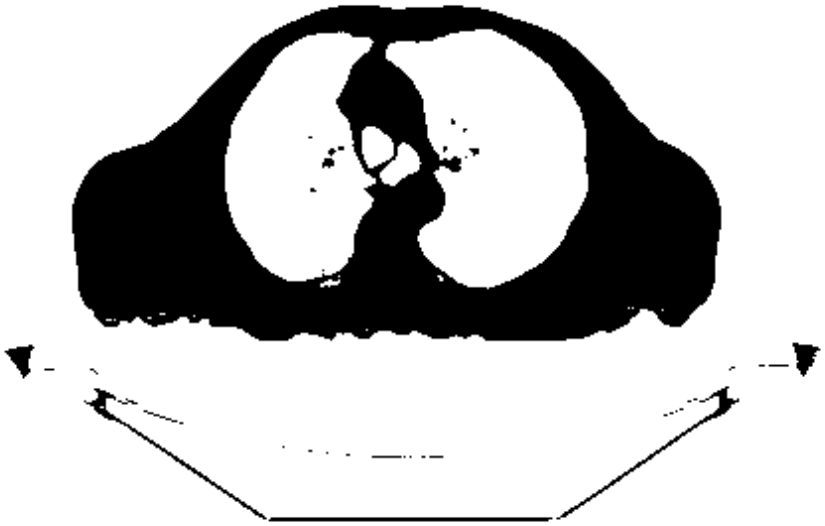

Figure 16 - Central slide inverted

Then, we remove other segmented elements in addition to the lungs with imclearborder (see figure 17) and fill in the gaps within the lung segmentation with imfill (see figure 18), at this command we have to indicate the 'gaps' parameter.

Figure 18 - Mask with imclearborder()

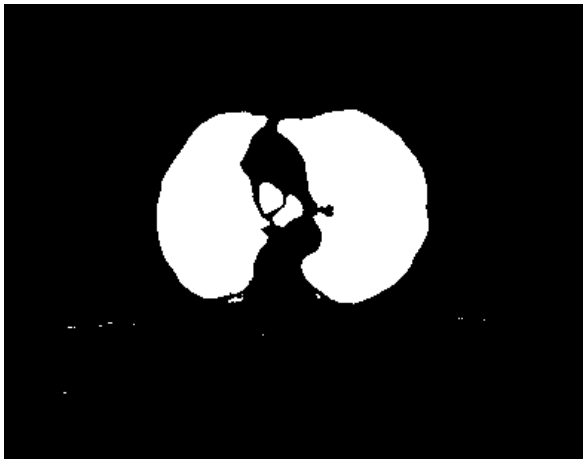

Figure 17 - Mask with imfill()

Finally, we will modify the morphology of our mask to smooth the edges of the lung segmentation. For this we create two intermediate variables, radius and decomposition with the values 3 and 0, respectively, that we will introduce by parameter to the strel command. Strel creates a disk-shaped structuring element, where it specifies the radius and specifies the number of line-structuring elements used to approximate the shape of the disk. This element is the one used to erode our mask with the imerode command. See figure 19.

Figure 19 - Mask with imerode()

Once this is done, we can create our new image with the mask for the XY section applied. See figure 20. We use the symbol "~" that corresponds to the logical NOT operation, setting as 1 all the values of our original section that do not match the mask created.

Figure 20 - Final mask

To create this mask using the Image Segmenter application, the steps would be as follows. We open the application from the MATLAB Apps toolbar or using the imageSegmenter command, specifying a 2-D segment as an argument, imageSegmenter (XY) in this case since it is the segment we are dealing with. To start the segmentation process, we click on Threshold to open the lung slice in the Threshold tab. In the Threshold tab, we select the Manual Threshold option and move the Threshold slider to specify a threshold value that achieves good segmentation of the lungs. We click on Create mask to accept the threshold and return to the Segmentation tab.

In the application, we invert the image of the mask so that the lungs are in the foreground (Invert Mask), we remove other segmented elements in addition to the lungs (Light Edges) and we fill the holes within the lung segmentation (Fill Holes). Finally, we use the Morphology option to smooth the edges of the lung segmentation. In the Morphology tab, we select the Erode Mask operation. After performing these steps, we select Show Binary and save the mask image to the workspace.

4.3.2. Image Processing – 3D VOLUME

This algorithm was developed considering the advantage of DICOM files since they can be worked with in 3D. In this case the files are evaluated as 3D structures calculating volumes directly.

Although this algorithm is simpler, it also has certain drawbacks since it is not as precise and exact as the previous one. Despite this, how it works will be briefly explained.

Both the starting form and the processing of all patient data as a whole is the same as in the previous algorithm. The main difference lies in the "LUNG" function, which is why we will explain it. The evaluation script has not been developed in this case as it is not an effective algorithm.

4.3.2.1. LUNG

This function is the one that analyzes and processes the CTs one by one. To this function we put the path_in parameter, that is, the directory of our DICOM file and it returns the volume of the lungs by parameter in the variable Vol. See figure 21.

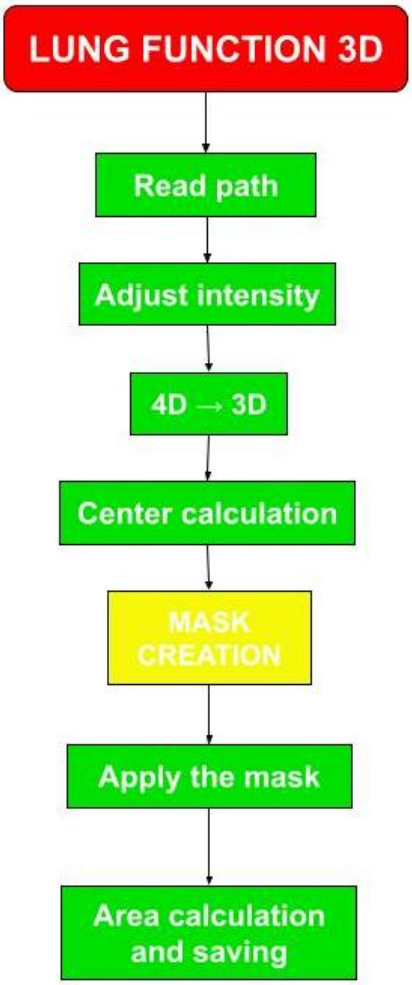

Figure 21 - Lung function flow chart 2D

The first thing we do is read the DICOM file from the directory with the dicomread command and save it in the info variable. Then, we use the im2single method, which converts the intensity image I to single, rescaling the data if necessary and with the imadjustn method we adjust the intensity values of the image. By default, saturates the bottom 1% and top 1% of all pixel values. This operation increases the contrast of the output image.

The last step before starting to segment the lungs is to go from our 4D image to a 3D image. To do this, we assign the value 1 to the third dimension of our 4D image and then we use the squeeze command to eliminate this dimension since this command eliminates those dimensions that are equal to 1. Once we have our file in 3D, we can use the volumeViewer command to visualize our structure in the workspace.

So far, the steps are the same as in the 2D algorithm. The difference is that now a 3D mask will be created. This mask is created by merging two 2D masks on different planes. Two central sections, longitudinal and transversal, are also used to create these masks. The mask creation process is done with the mask function, described above.

When applying the 3D mask to the structure, no loop is necessary. It is applied directly using the active contour technique. Active Contours is a region growth algorithm that requires initial seed points.

Now we perform the calculation of the volume of the segmented lungs. We use the regionprops3 function with the "volume" option to calculate the volume of the lungs. VolumeLungsPixels will then be a structure with the values of the volumes of our image once we have applied the mask. As images can have noise, we will order this structure to remove only the two largest volumes, which correspond to our two lungs. To order the structure we have to pass it to table format, we sort it in descending order and return it to structure.

We will save our total volume. We will first check that the VolumeLungsPixels vector is not empty and then we will save it. If the vector VolumeLungsPixels is empty, we will assign the value NaN to the variable Vol.

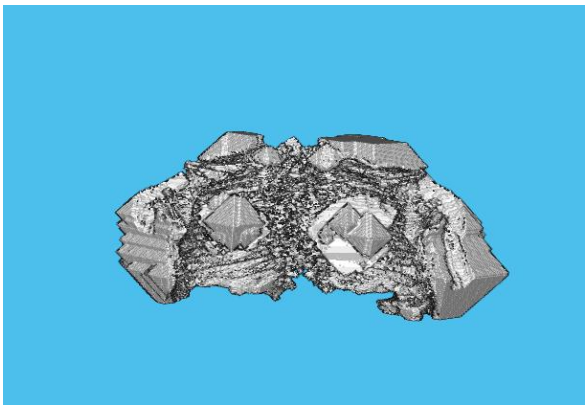

Figure 22 - Final Volume with 3D algorithme

The figure 22 is the volume obtained from the same data as the 2D algorithm test. We can see that it is a less exact volume. This will be discussed in the results section.

4.4. Evaluation

As we have discussed previously, the results have been stored in an Excel file called IPACOVID_Reus_modified_2D. To evaluate this data, a new Matlab script called evaluation has been created. In this script the excel file has been opened using the xlsread command, in which the name of the file with its location is entered by parameter, saved in the filename variable.

Various types of representations will be made to be able to evaluate different variables that must be considered in relation to lung volume.

First, a general boxplot has been carried out to see the trend of the values obtained, that is, the trend of lung volumes.

A linear graph has been made that shows the evolution at the volumetric percentage level of all the patients treated in the study. Before making this graph, the volumetric percentages have been calculated. For this, 100% has been assigned to the basal volume and the percentages of the monthly and weekly volumes have been calculated with respect to it.

Two graphs have been represented showing the trend of the mean of these percentages, also showing their standard deviation. This graph has been made in a general way with all patients and has also been made by differentiating the patients by sex to check if there is any relationship between sex and the effect of treatment with LD-RT.

Finally, two scatter plots were performed, one with PAFi and the other with SAFi to check if there is any relationship between these values and the increase or decrease in lung volume. These scatter plots have been made using external functions belonging to the Matlab community.

5. Results

Once the algorithms used to perform the clinical evaluations have been exposed and explained, we will see the code results and clinical results of this project. Within the results of the algorithms, we can differentiate two main ones. The first would be the algorithm previously exposed, which has been the most optimized that has been obtained and the second would be a 3D image processing algorithm.

5.1. 2D-Algorithm with previous section

5.1.1. Algorithm

In this first algorithm, the one explained above, it has been possible to obtain an image processing algorithm that allows us to process, calculate and evaluate the lung volume of the patients. This algorithm processes our CT images section by section, that is, we treat each image as a single 2D image and then calculate its area. By calculating the lung area in all the slices of our computed tomography, we obtain the total volume.

The total volume obtained is stored and evaluated in voxels as it is used for internal evaluations of the program. For the clinical part of the project, this data can be transformed into cubic liters. To do this, we must obtain information on the density of the sections of the tomograph used to take the samples. As this is an ongoing study, it has not been considered.

This algorithm has the advantage that it evaluates and processes each image individually, that is, creating the images individually for each one. This allows us to have a more accurate and precise algorithm.

The general 3D structure obtained is what we can see in the figure 23. It can be seen that it is a 3D structure that only contains the lungs. In some of the final sections there is part of the windpipe but as when storing the volumes only the two largest volumes are stored, thus avoiding storing these volumes

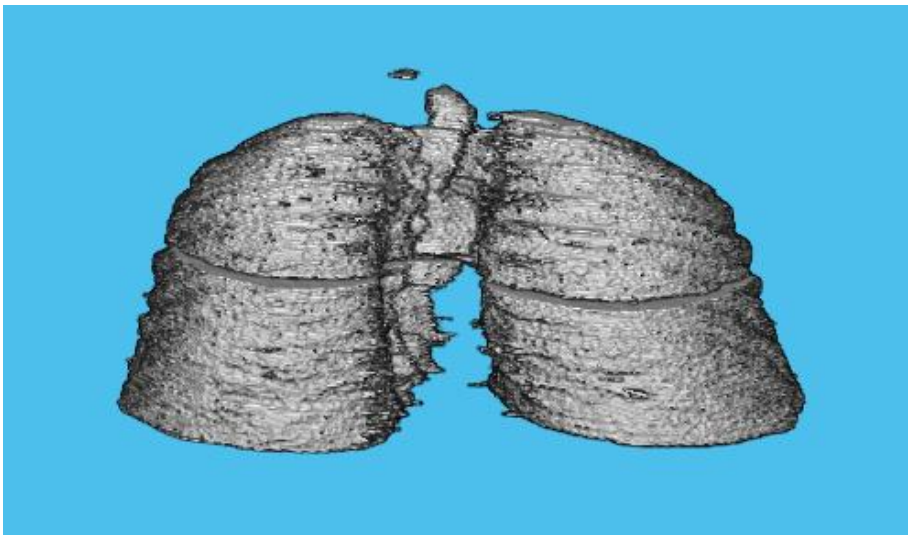

Figure 23 - Final Basal Volume Example with 2D algorithme

We will see below the longitudinal and cross sections of the structure in 3D (see figure 24 and 25). These images have a high contrast so we can better appreciate if there is any structure external to the lungs, but it can be seen that this is not the case.

Figure 25 - Longitudinal section of the structure represented in figure 23

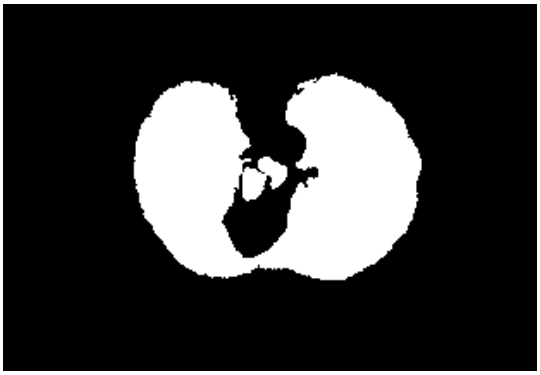

Figure 24 - Cross section of the structure represented in figure 23

5.1.2. Improvements

Despite the fact that this is the most efficient and accurate algorithm that has been obtained, it has some disadvantages. Its main disadvantage is the processing time of some functions. This is still a problem even though an attempt has been made to fix it by using different functions instead of a single script.

Separate operations have also been placed outside the loops since if the code is not evaluated differently with each iteration of the for or while loop, it is better to move it outside the loop to avoid redundant calculations.

As we have described before we see that this algorithm is based on the comparison of the similarity of the consecutive masks. One of the possible improvements that can be applied would be to change this comparison. To improve its efficiency, instead of only comparing the similarity of these images, the location of the masks in the plane would also be compared. A failed example of CT processed with this algorithm is shown in the annex.

5.2. 3D-Algorithm

5.2.1. Algorithm

In this second algorithm it also allows us to process, calculate and evaluate the lung volume of the patients. This algorithm processes the CT images as a total 3D structure, that is, we do not isolate each image as one, but we evaluate them together and then calculate their volume directly.

The total volume obtained is stored and evaluated in voxels as it is used for internal evaluations of the program. For the clinical part of the project, this data can be transformed into cubic liters. To do this, we must obtain information on the density of the sections of the tomograph used to take the samples. As this is an ongoing study, it has not been considered.

This algorithm has the advantage that it evaluates and processes the 3D structure without dividing it. This allows us to process the file in 3D and be able to take advantage of the different methods and functions to work with volumes that Matlab has. It is also a more visual algorithm since the calculated volume can be accessed more easily, thus facilitating the interpretation of the data by the medical staff.

The general 3D structure obtained is what we can see in the figure 26. You can see that it is a 3D structure that not only contains the lungs, but also contains structures external to them. We will discuss this in the next section.

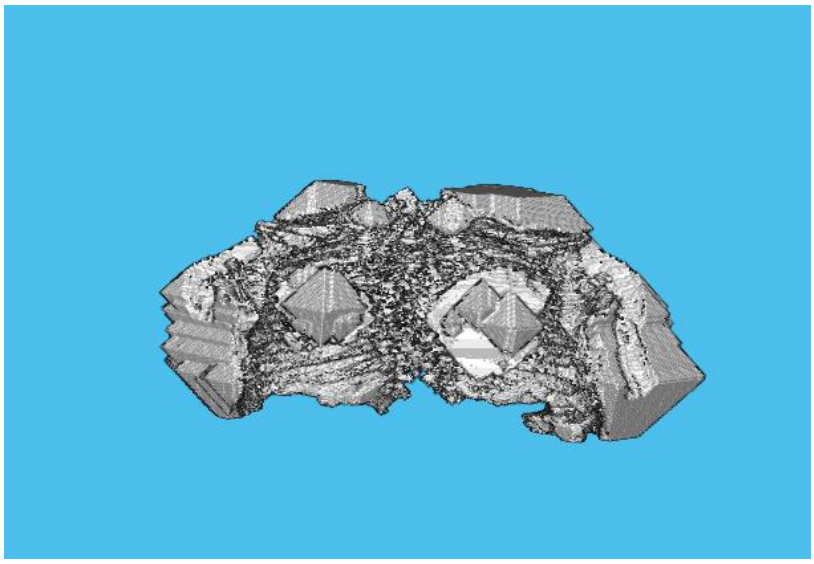

Figure 26 - Final Basal Volume Example with 3D algorithme

The longitudinal and transverse sections of the volumetric structure can be seen in the following figures. The image of the lung here is clearer.

Figure 28 - Longitudinal section of the structure represented in figure 26

Figure 27 - Cross section of the structure represented in figure 25

5.2.2. Improvements

This algorithm has been discarded due to its problems and inaccuracies. With the previous images you can see these external structures. These could be isolated from the lungs if we simply select those larger volumes as in the algorithm above. This has been tried but it is not possible to solve it in this way since in many areas these structures are connected to the lung volumes, therefore they are evaluated as a single structure. In the transverse and longitudinal sections, it can be seen that the volumes are surrounded by external structures that do not correspond to the lungs. It can also be seen that these structures are connected to the lungs so they cannot be easily ruled out.

Another option so that these structures are not a problem is that they are constant within the same patient. In this case, even if they increased the lung volume, they would increase the same amount in the three CTs evaluated and since the purchases are made within the same patient, it would not pose any problem. In our case, this is not the case since these structures depend on the position of the patient when performing the CT and this differs between one CT and another.

The best solution for this is to apply a volume mask that only selects the main structure in it. To improve this algorithm, the creation and application of the 3D mask can also be made more efficient and precise so that when applying it, it is more exact and faithful to the real volume.

5.3. Clinic results

Within the two algorithms developed, only one of them has been considered efficient and precise enough to carry out the evaluation of the data obtained. Before commenting on these results, we have to see in the following table the sample of data with which we have carried out the evaluations.

In this table we can see the number of patients whose CTs have been evaluated in the different periods. We also see the mean values of SAFi and PAFi as well as the mean value of volume obtained.

	BASAL	WEEK	MONTH
Number of Patients	31	31	24
SAFi Value	293.13	400.93	459.52
PAFi Value	259.16	351.01	474.42
CT Volume Voxels	712594	602891	585850

Table 2 - Table on the number of CTs and mean values of volumes, PAFi and SAFi

We will now analyse the different graphs obtained with the evaluation script. The first graph shown is a boxplot where the values of lung volumes have been represented in voxels in relation to the CT to which they correspond. A box plot (also known as a "box-and-whisker plot" or "box plot") is a standardized method of graphing a series of numerical data through its quartiles. In this way, the box plot shows at a glance the median and quartiles of the data, 1 being able to also represent the outliers of these.

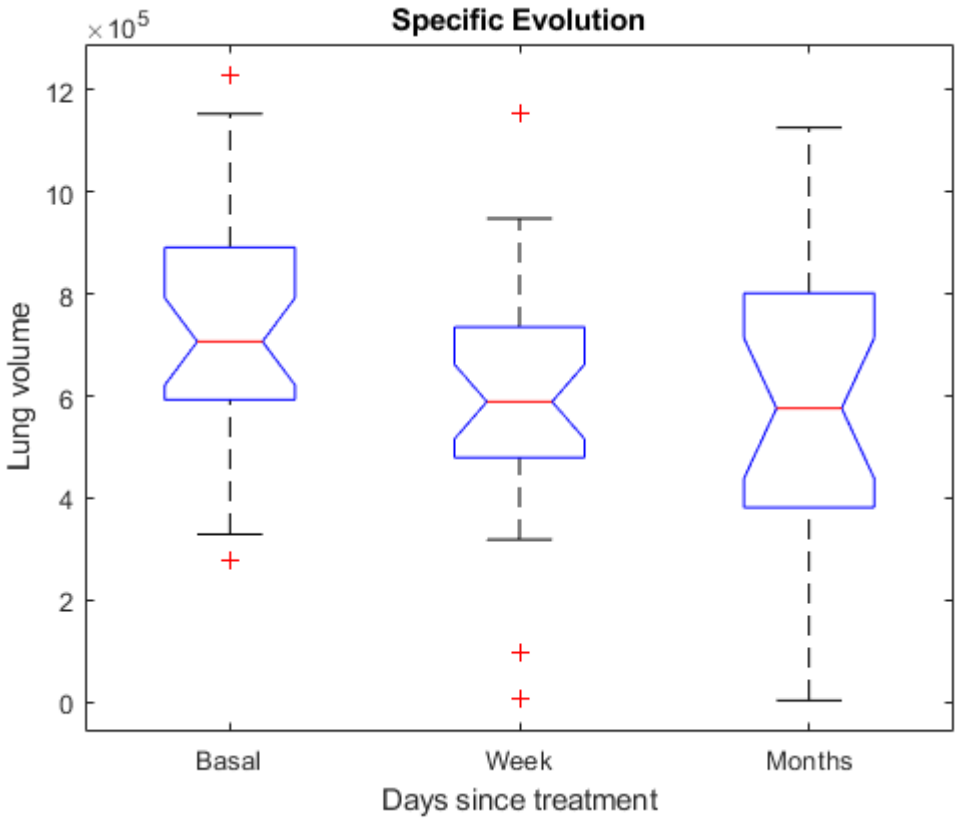

Figure 29 - Boxplot Specific Evolution

One of the main hypotheses to check is the anti-inflammatory efficacy of LD-RT. For this, the main variable to check is the lung volume of our patients, comparing whether there are differences in volumes between the Basal CT, the CT of the week and the CT of the month. For this, this boxplot has been used, grouping all the volume values in voxels.

It can be seen in the figure that although there are some important outliers, the mean volume decreases as the days after treatment increase. With this simple result, it can be stated that the assumption that LD-RT produces anti-inflammatory effects is a true hypothesis.

Within this graph you can extract different information. One of the most obvious is the median. The median is represented by the line on the box. The median is a common measure of the centre of the data. Half of the observations (the volumes) are less than or equal to the value and half are greater than or equal to the value. It is a good indicator of the decrease in volumes as it can give us a general idea.

Another important piece of information is the interquartile range table. Before defining this we must know that quartiles are values that divide a data sample into four equal parts, it can be seen in the following table. They are used to quickly assess the spread and central tendency of a data set. The interquartile range box represents the middle 50% of the data. Shows the distance between the first quartile and the third quartile (Q3-Q1).

Quartile	Description
1º Quartile (Q1)	25% of the data is less than or equal to this value.
2º Quartile (Q2)	The median. 50% of the data is less than or equal to this value.
3º Quartile (Q3)	75% of the data is less than or equal to this value.
4º Quartile (Q4)	The distance between the first 1st quartile and the 3rd quartile (Q3-Q1); in this way, it covers the central 50% of the data.

Table 3 - Table of Quartile description

Before the representation of the following graph, the volume percentages of each patient for each CT have been calculated. For this, the basal volume, or initial volume, has been indicated as 100%. As a function of this initial volume, the other two puminous volumes have been calculated in percentages.

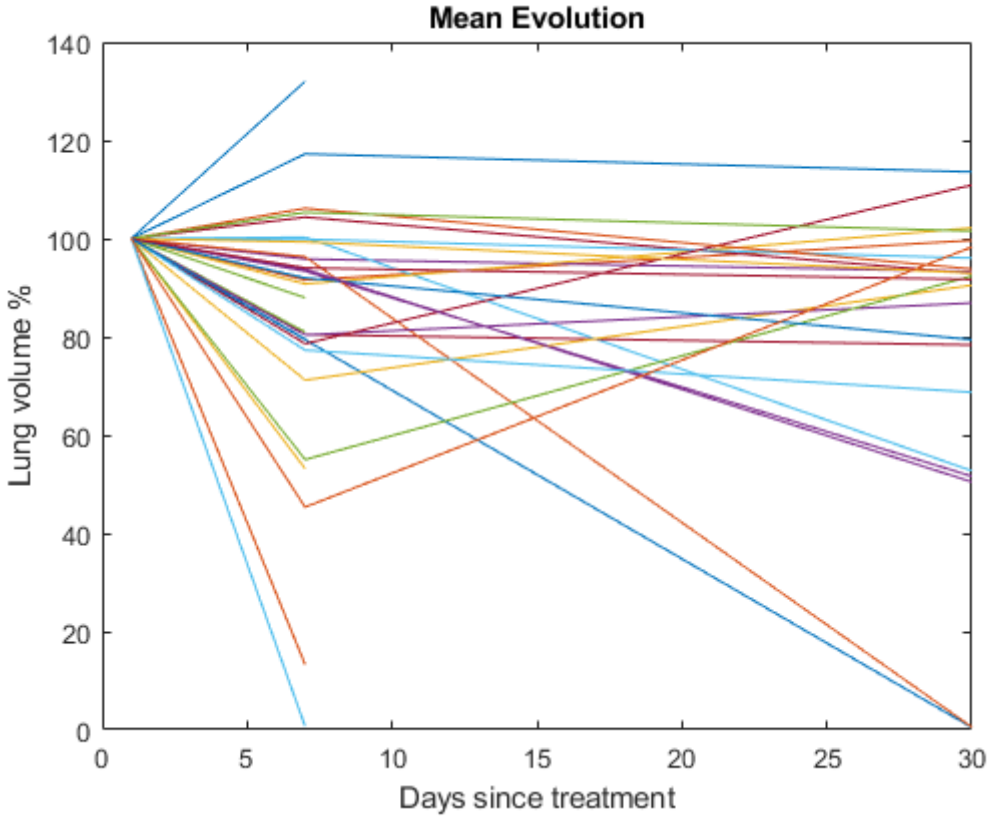

Figure 30 - Percentage Evolution Linear Plot

The following graph represented is a linear graph that represents these volumes. Each line corresponds to a specific patient. It can be seen that there are quite a few lines that do not continue until the end, this is because the patients to whom these representations correspond have not survived until the month after the treatment, so we do not have the CT scan of the month.

It can be seen that despite the fact that there are some patients who do not comply with what is expected, the majority do present a decrease in lung volume. We can also see that it is not a constant decrease, that is, there are patients in whom the anti-inflammatory effect is greater and others in whom it is less. This may be due to patient characteristics, either sex or age, which we will evaluate in the following graphs.

The next graph to analyze is a regression line graph. In this graph we show all the volume data of the patients without making distinctions between them. The relationship between the percentage of voumen calculated before with the treatment day to which said CT corresponds is shown. In this case, it can be seen more clearly how the tendency of the lung volume is to decrease once the treatment with LD-RT has been applied.

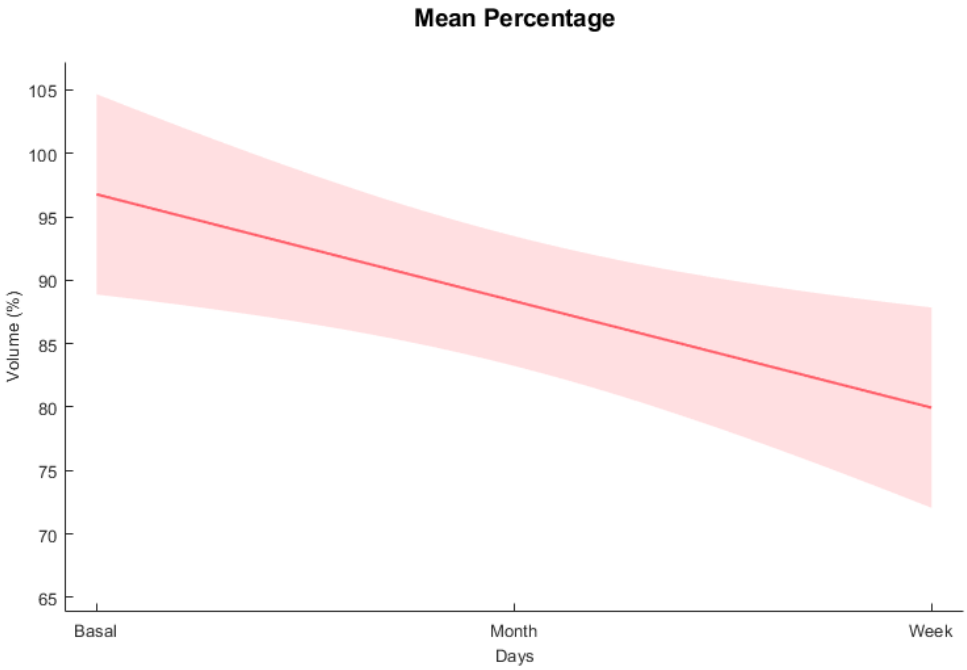

Figure 31 - Mean Percentage plot

If we apply this same graph but separate our samples by sex (female gender in red and male gender in blue, as can be read in the legend), we obtain the following graph.

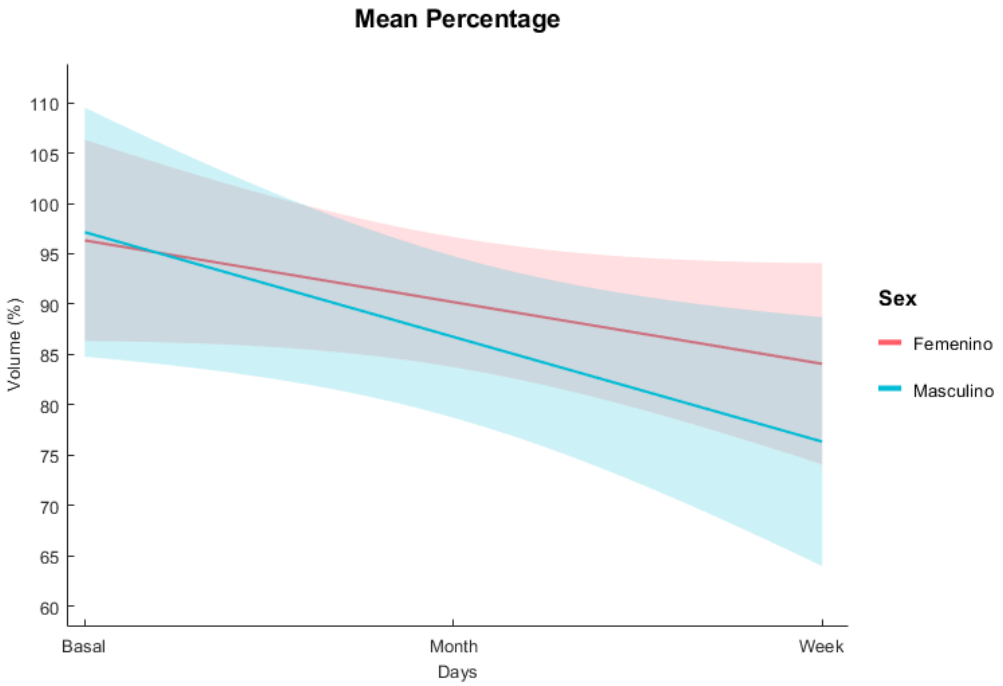

Figure 32 - Mean Percentage plot divided by sex

In the previous graph it can be seen that although both sexes present a considerable decrease in volume, the male sex presents a greater decrease and therefore a greater anti-inflammatory effect. We can also observe that this difference in volumetric decrease is more noticeable in the CT of the month than in the CT of the week.

In the clinical setting, this inequality could be a key aspect when selecting more patients for the study. If we consider the collapse situation in which the World Hospitals found themselves during the highest peaks of the waves of the pandemic, the choice of the appropriate treatments for each type of patient was key to avoid the loss of time and resources both of medical personnel and infrastructures. The distinction by sex when applying certain treatments could be a great advantage in these cases. Male patients would be prioritized for this type of treatment with LD-RT since they have shown a greater improvement in lung inflammation by means of RT, being able to focus female patients on other types of treatments.

The following chart is a scatter plot. This is a type of mathematical diagram that uses Cartesian coordinates to display the values of two variables for a data set. The relationship between lung volume and PAFi value is represented with this scatter plot.

The PAFi Index is one of the most widely used oxygenation indices and refers to the relationship between arterial oxygen pressure and the inspired fraction of oxygen (PaO2 / FiO2). The lower the PAFi, it means that there is a worse gas exchange. In general, it is considered that below 300 there may be an acute lung injury and below 200 there may be an acute respiratory distress syndrome. If we apply this to our graph, a decrease in lung volume must be related to a high PAFi index.

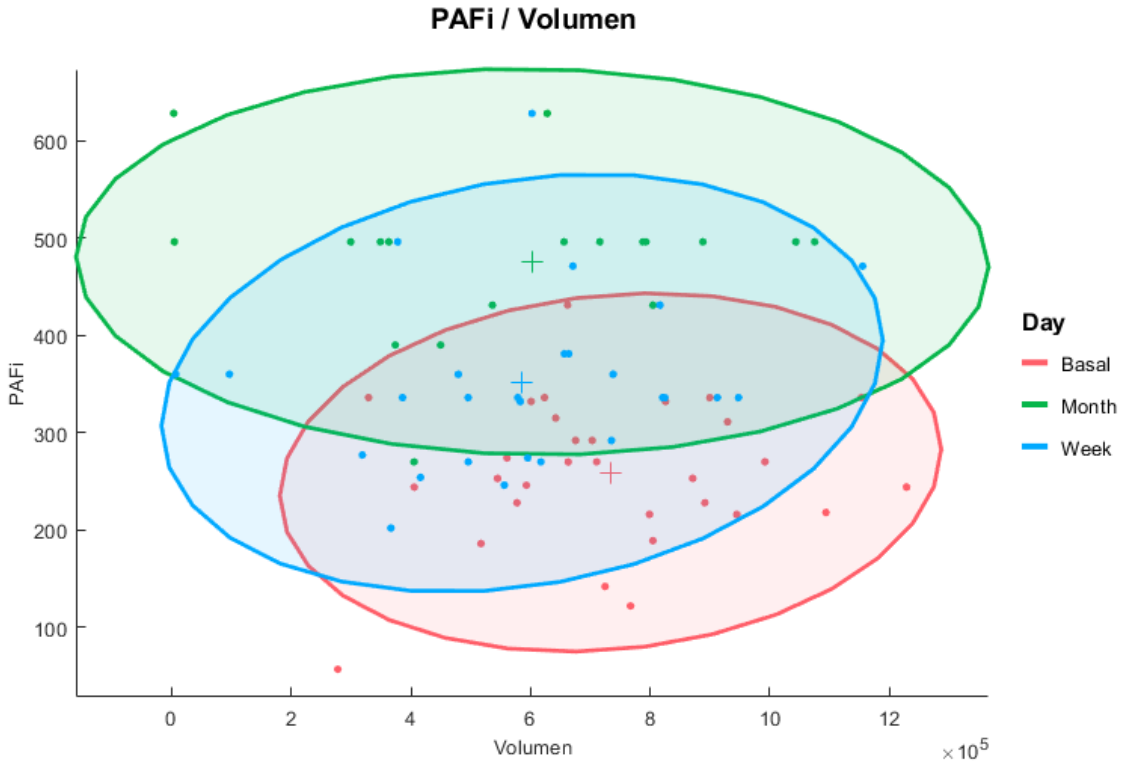

Figure 33 - PAFi/Volume Scatter plot

In our graph, the samples have been differentiated by the day of the CT scan (baseline, week or month) by making groupings divided by colors. We can see that those samples that correspond to the CT scan of the month, which tend to have a lower lung volume and therefore more normal, have a higher PAFi index. Following this dispersion, the CT values for the week have a medium PAFi index and those of the baseline CT have a very low PAFi index.

The last chart is also a scatter plot but in this case we will use the SAFi index in reaction to volume. The SaFi index (SaO2 / FiO2) is the ratio between the transcutaneous oxygen saturation and the inspired fraction of oxygen.

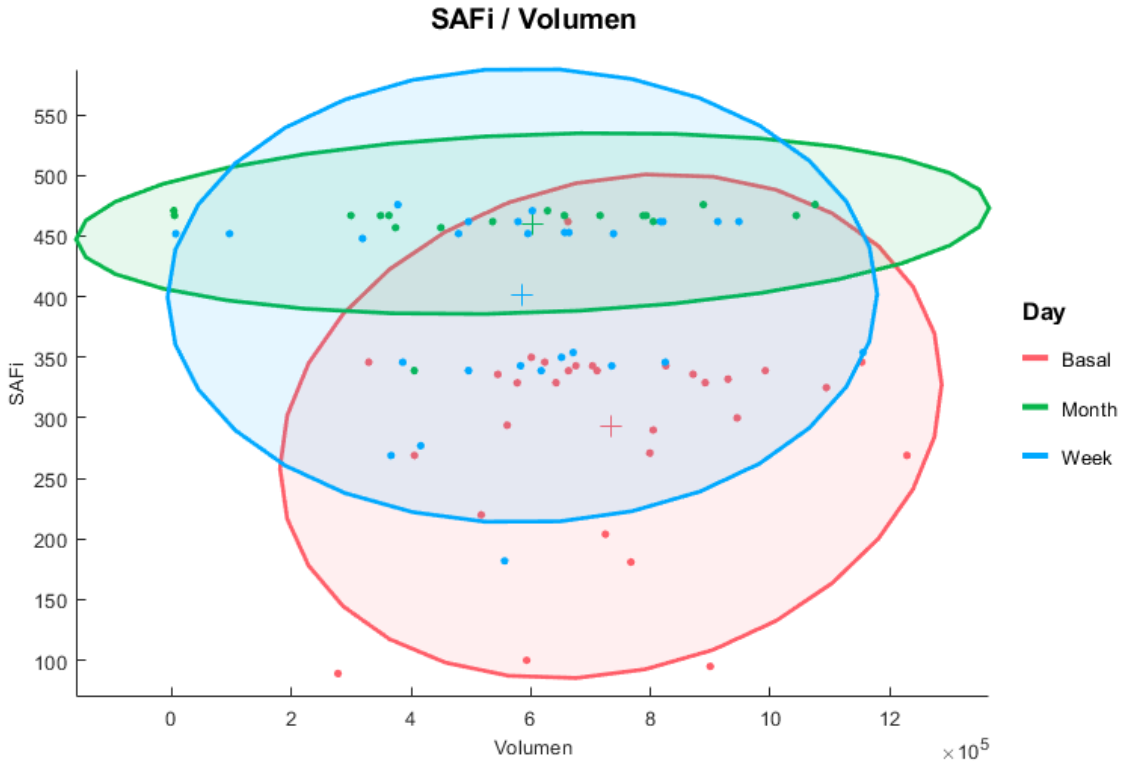

Figure 34 - SAFi/Volume Scatter plot

We see that in this case there is a greater overlap between the values when they correspond to the monthly and weekly CTs. We must bear in mind that some of the patients used for the study do not have a monthly CT scan because they died before the month of treatment. In the case of these patients, it is likely that they reached their maximum SAFi value during the first week but later died from causes other than lung inflammation.

In order to have this clearer, the following table is attached that collects the data of the deceased patients before the month of treatment together with their causes of death.

Patient	Death day after LD-RT	COVID-19	Age	Reason
7	7th	Yes	88	Acute respiratory distress secondary to COVID-19
8	7th	No	74	Septic infection of unknown origin without response to empiric antibiotic administration
9	8th	No	73	Broncho aspiration, having a subdural hemorrhage recent intervention.
10	11th	Yes	87	Acute respiratory distress secondary to COVID-19
11	12th	No	60	Severe worsening of his chronic renal failure under hemodialysis treatment
12	14th	No	55	Esophageal varices hemorrhage, having a known antecedent of enolic hepatic disease
13	25th	No	85	Severe pulmonary thromboembolism

Table 4 - Causes of death, from COVID-19 or other causes following low-dose radiation therapy (LD-RT)

6. Conclusions and Future Lines

6.1. Conclusions

The objective established before carrying out this work was the development of an algorithm capable of segmenting and evaluating chest CT images of coronavirus patients treated with LD-RT and evaluating them. This has been carried out by extracting volumes based on colour information and comparing them.

Once the algorithm has been implemented and the relevant tests have been carried out, it is verified that the algorithm fulfils its purpose:

- It is an autonomous system, since the parameters used are fixed for all the images, without any dependence on the input image.
- It succeeds in segmenting the lungs present in the images, giving fairly accurate results.

The following conclusions have been obtained from the study carried out:

- The developed system consists of three phases: image preparation, volume detection and evaluation.
- Evaluation using 2D images has proven to be the most efficient method compared to evaluating 3D images.
- Different correlations have been found between the volumetric data obtained and the data provided by the Hospital regarding the patients.

In view of the results obtained in this work, it can be stated that both the analysis of structures in 2D and 3D are powerful tools that can undoubtedly help in medical imaging, although certain improvements are necessary. We can also affirm that during the study carried out, clear evidence was obtained that LD-RT has anti-inflammatory effects; therefore, the initially proposed objectives have been achieved, being demonstrated with the results obtained experimentally.

6.2. Future Lines

This project opens the doors to future lines of work with which even better results could be achieved. A fundamental work is to increase the sample of the study population, in this way a more representative sample of the population can be achieved, and the classification models have more information to refine their precision.

This is a difficult task if we treat the project as a specific study of COVID-19, as this disease is currently in decline. To achieve this, then we would have to approach the project in general terms, such as the evaluation of CT images in patients with pneumonia.

Another option would be to focus the algorithm on the oncological field since it is a field in which medical imaging is fundamental. An example in this field would be the evaluation of the response of lung tumours to different treatments. It could also be correlated with the clinical and respiratory tests of SAFi and PAFi.

On the other hand, other volume detection methods could be tried that could develop a system with higher performance. In the same way, the methods already created could also be improved, improving their sensitivity and effectiveness.

One way to improve this project would be to be able to study these structures through densities and textures in the image. The density of the lungs is largely related to improved breathing. For this reason, the densities could be evaluated to see if there is any relationship between the treatment with LD-RT.

7. Annexes

In this annex, the evaluations of the CTs of two different patients will be developed, one of them the patient treated previously and the other a patient whose CTs are not normal and are not evaluable by the algorithm.

7.1. Normal patient

For this development, the patient whose id is 915392 will be used. First, the baseline CT scan will be thoroughly analysed step by step and then the three volumes obtained will be compared. In the following figure you can see the 3D structure from which the evaluation starts.

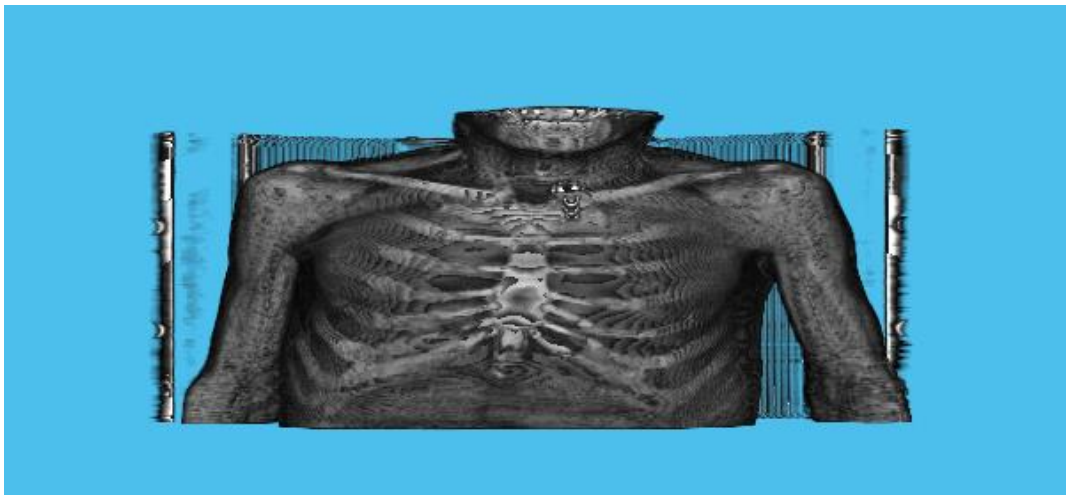

Figure 35 - 3D Raw Structure

The centre section is then selected, and your initial mask is created. You can see in the following figure the comparison between this section and its mask. This corresponds to section number 64 of 157.

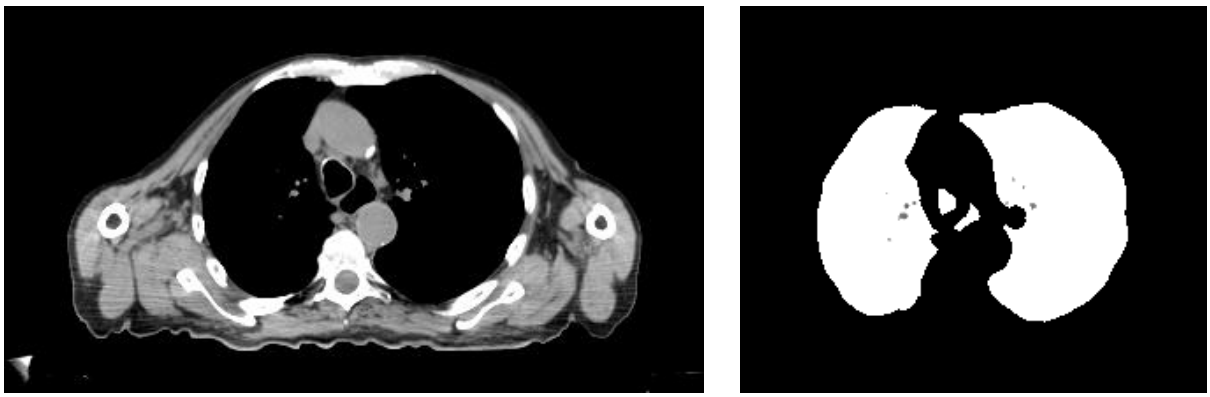

Figure 36 – Raw central cut and with its mask applied

In the following figures we will see the evolution of these masks along the upper and lower half of the baseline CT scan of our patient until the algorithm considers that there are no more lungs in the image. The top half is displayed first, then the bottom half. We will also see a table with the area data in pixels and the indexes of similarity between the sections.

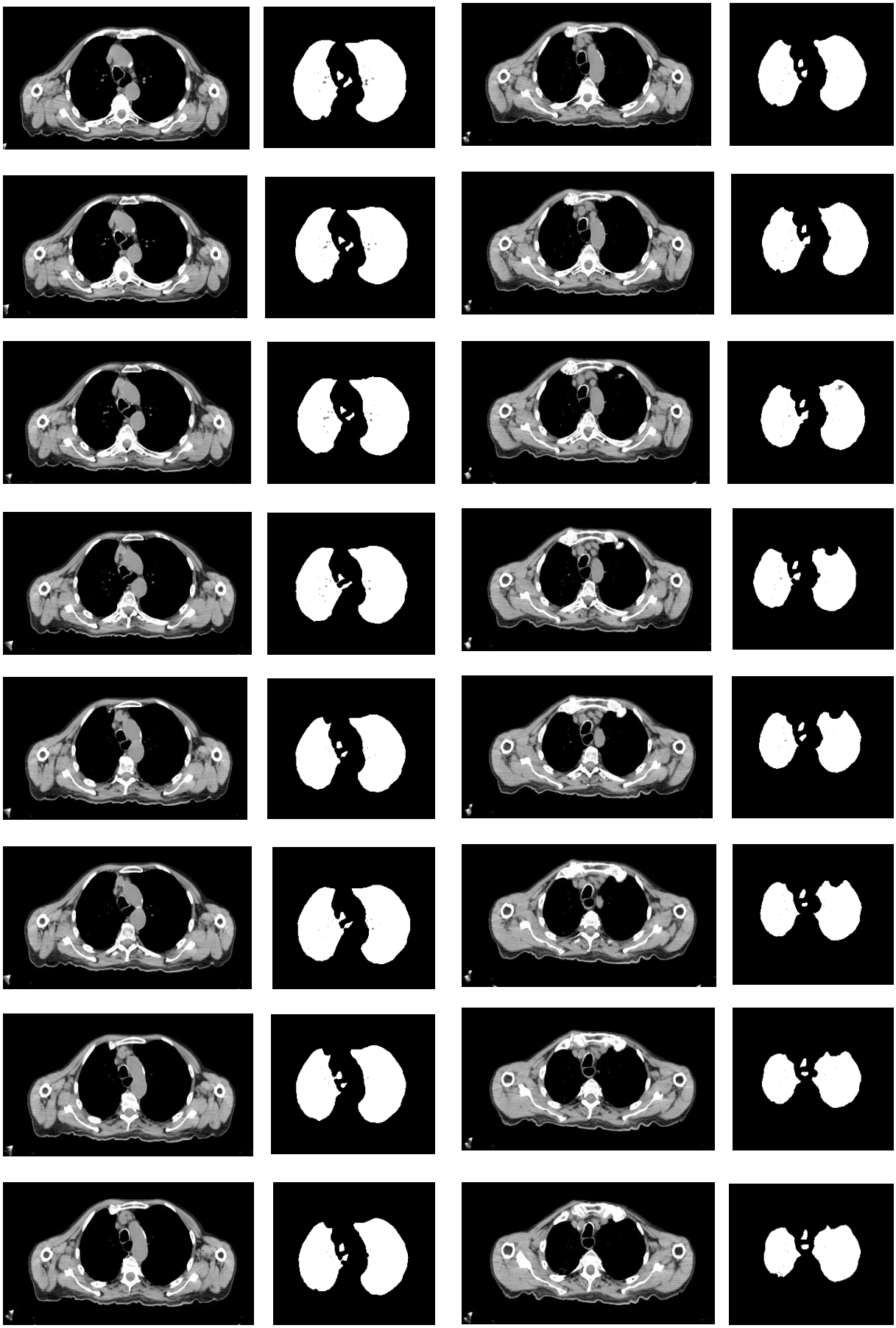

Figure 37 - raw top cuts and with their masks applied 1/2

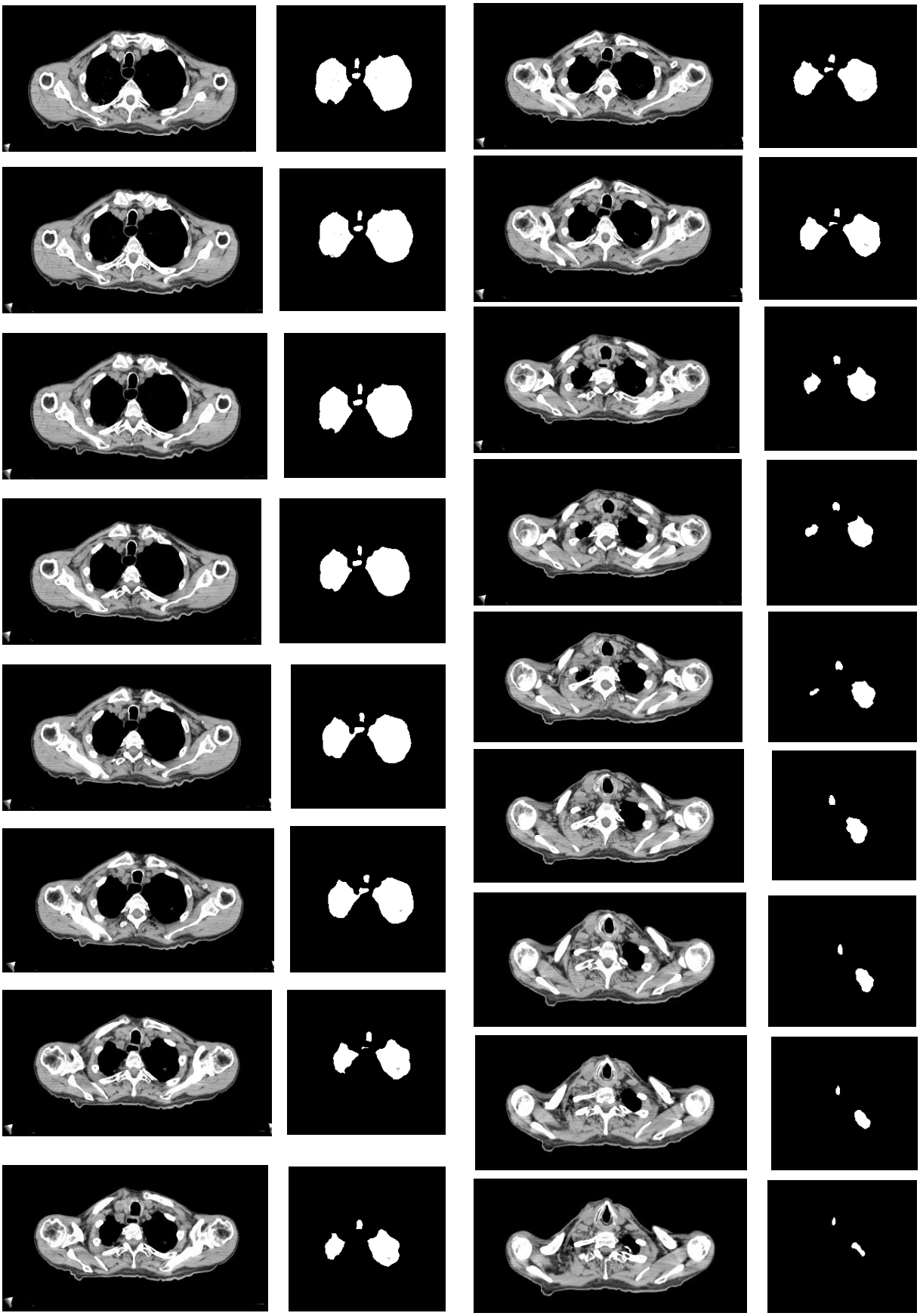

Figure 39 - - raw top cuts and with their masks applied 2/2

We will now see a comparative table with the area in pixels, and the similarity of the section with the previous one.

Section	Area (Pixels)	Similarity	Section	Area (Pixels)	Similarity
64	16313	-	46	7922	0.9565
63	15532	0.9726	45	7135	0.9569
62	15105	0.9799	44	7089	0.9587
61	15023	0.9800	43	6670	0.9473
60	14629	0.9779	42	6010	0.9447
59	14560	0.9793	41	5337	0.9273
58	14085	0.9789	40	4684	0.9224
57	13619	0.9808	39	4006	0.9066
56	13247	0.9777	38	3252	0.8976
55	13056	0.9764	37	2784	0.8812
54	12549	0.9654	36	2138	0.8541
53	11781	0.9613	35	1579	0.8467
52	10986	0.9418	34	1416	0.8365
51	9747	0.9551	33	1257	0.8470
50	9737	0.9526	32	842	0.8076
49	9342	0.9497	31	520	0.6226
48	8843	0.9562	30	-	0.3861
47	8522	0.9547			

Table 5 - Data of the processing of the upper half of the CT (section, area, similarity with the previous section)

In the table above we can see that the index of similarity between the section itself and the previous section is normally quite high, that is, the masks of both sections are very similar. However, in the last section treated (section number 30) the similarity index is 0.3861. This value is lower than the minimum similarity value that we have assigned, so we no longer consider this section as part of the lungs and it is discarded. For this reason, the area of this section is not calculated.

It can be seen that we do not have the similarity index calculated for section 64, which is the central section, since it does not have a previous section.

Now we will see the same procedure with the lower half of the torso. We will start from section 64, the central section, but in this case, we will not calculate the area of this section since it is previously calculated. If the area of this section were recalculated again, there would be an accuracy failure.

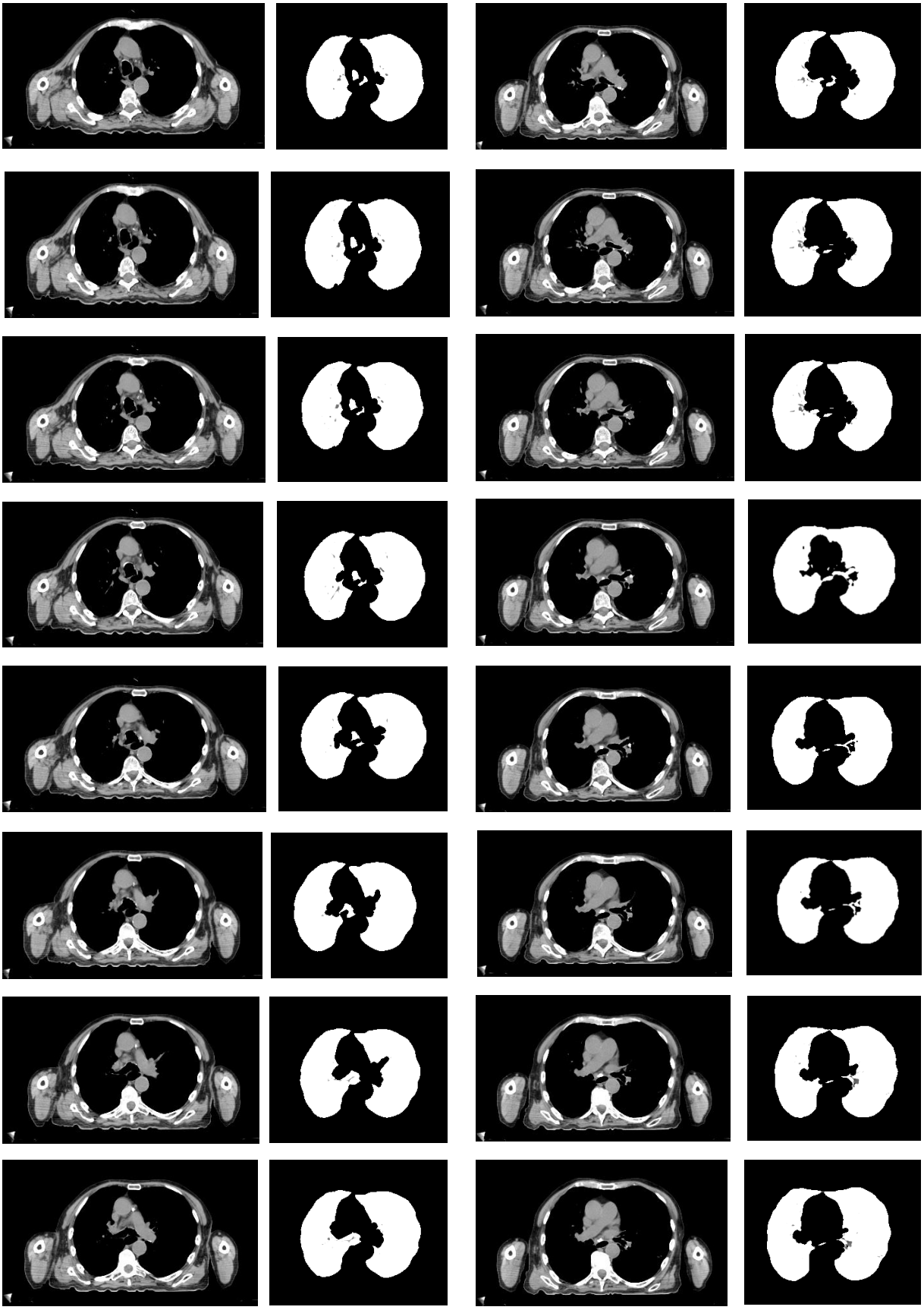

Figure 40 - Undercuts raw and with their masks applied 1/4

Figure 41 - Undercuts raw and with their masks applied 2/4

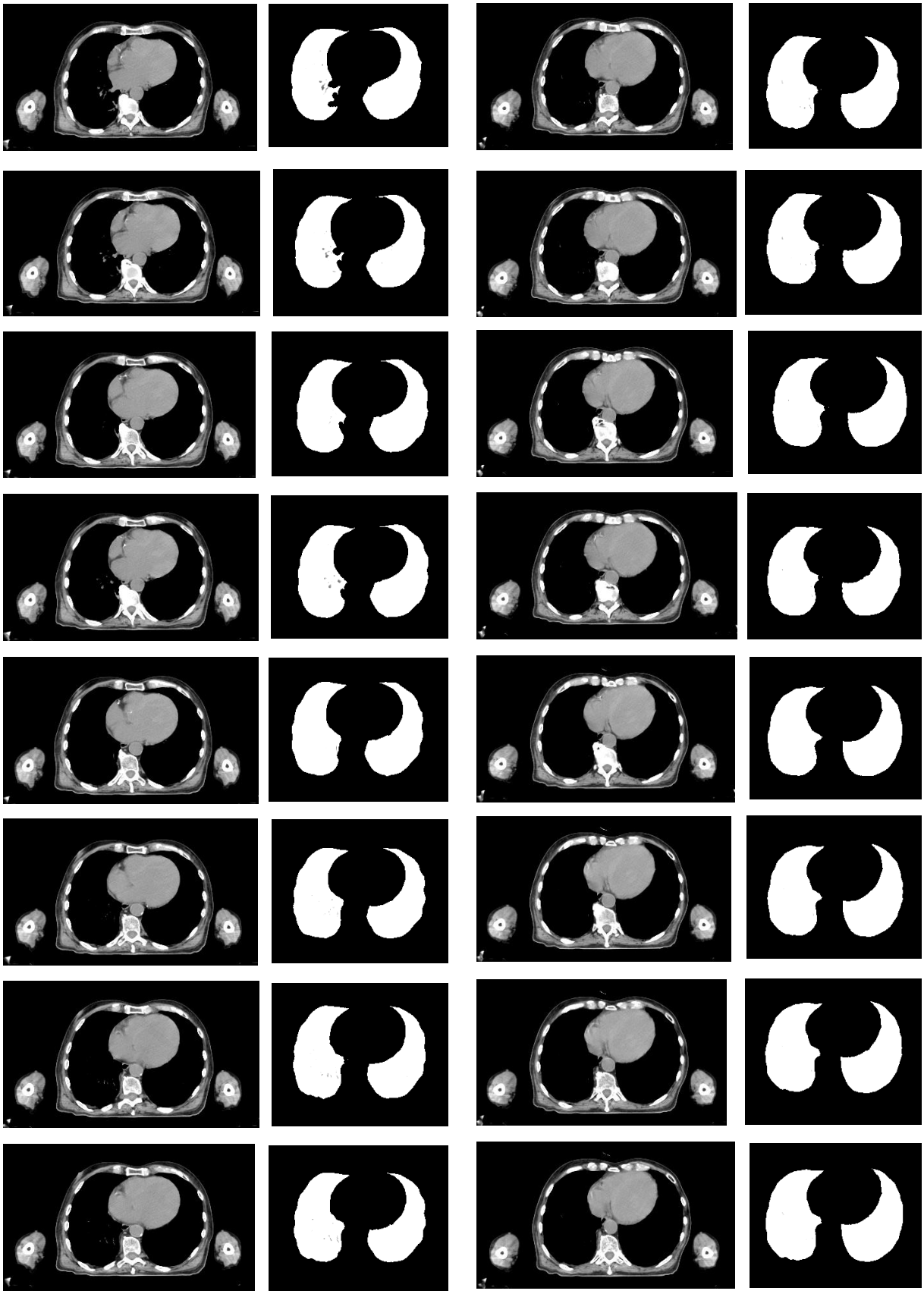

Figure 42 - Undercuts raw and with their masks applied 3/4

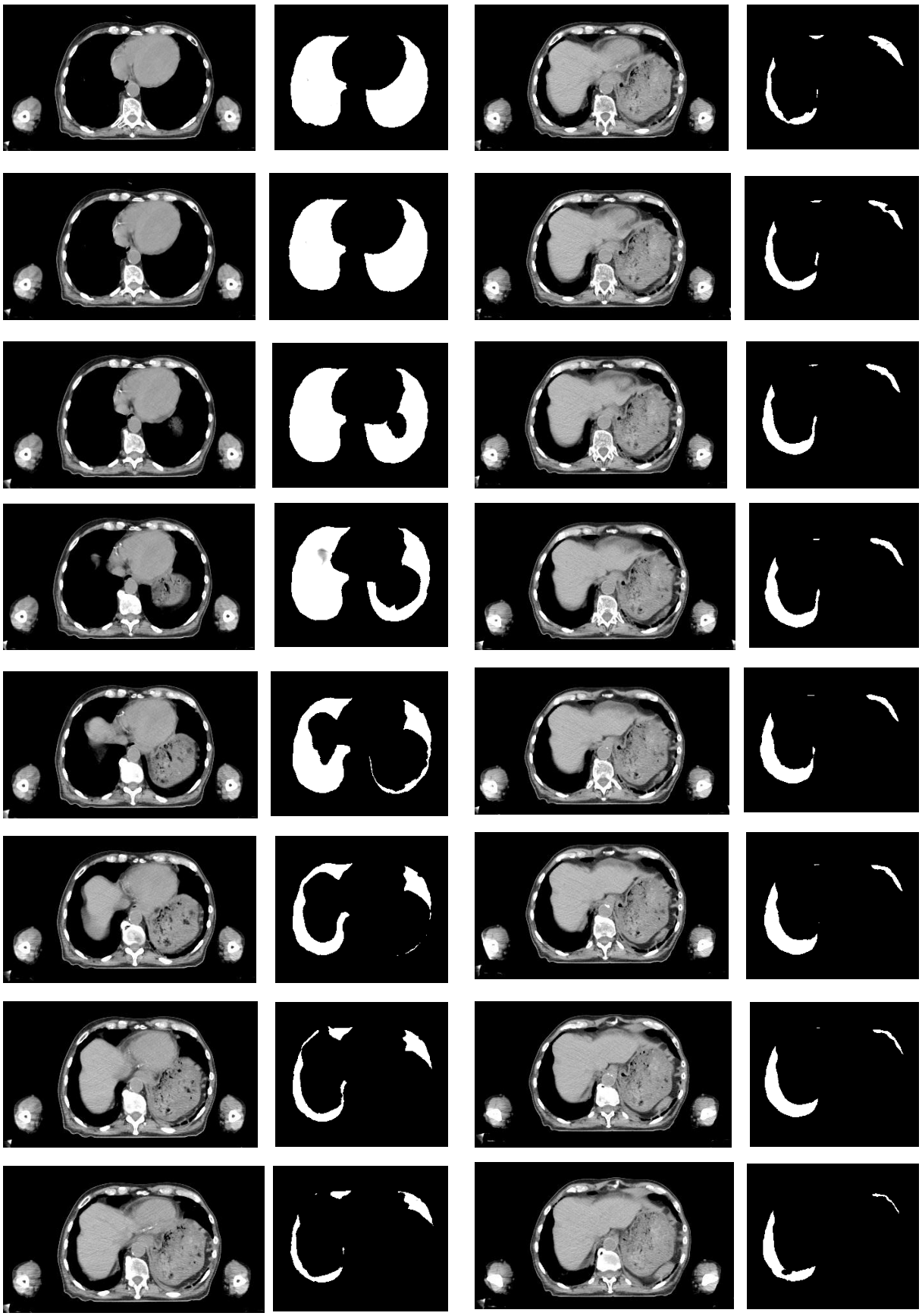

Figure 43 - Undercuts raw and with their masks applied 4/4

Section	Area (Pixels)	Similarity	Section	Area (Pixels)	Similarity
65	16721	0.9757	99	16850	0.9830
66	17105	0.9774	100	16874	0.9843
67	17489	0.9789	101	16549	0.9864
68	16844	0.9792	102	16677	0.9815
69	17771	0.9790	103	16301	0.9808
70	17480	0.9781	104	16453	0.9828
71	17587	0.9739	105	16026	0.9849
72	17335	0.9756	106	16269	0.9898
73	17494	0.9781	107	16274	0.9898
74	17119	0.9807	108	16124	0.9880
75	9412	0.8817	109	16210	0.9843
76	9967	0.9823	110	16381	0.9856
78	17528	0.8665	111	16507	0.9865
79	17769	0.9809	112	16877	0.9870
80	17810	0.9786	113	16849	0.9871
81	18251	0.9781	114	17337	0.9911
82	18490	0.9725	115	17971	0.9905
83	18561	0.9817	116	17092	0.9620
84	18622	0.9752	117	15863	0.9081
85	18641	0.9744	118	11863	0.7845
86	18030	0.9806	119	7398	0.7437
87	18187	0.9803	120	5948	0.7696
88	17955	0.9740	121	3960	0.7828
89	17508	0.9564	122	3628	0.8585
90	17094	0.9725	123	4511	0.8020
91	16985	0.9739	124	4765	0.8774
92	16662	0.9786	125	5027	0.9178
93	16383	0.9733	126	5180	0.9374
94	16501	0.9770	127	5030	0.9500
95	16174	0.9744	128	4081	0.9336
96	16474	0.9800	129	3613	0.8450
97	15992	0.9818	130	-	0.5178
98	16837	0.9763			

Table 6 - Data of the processing of the lower half of the CT (section, area, similarity with the previous section)

In the table above we can see that the similarity index between the section itself and the previous section is usually quite high, that is, the masks of both sections are very similar. However, in the last section treated (section number 130) the similarity index is 0.5178. This value is lower than the minimum similarity value that we have assigned, so we no longer consider this section as part of the lungs and it is discarded. For this reason, the area of this section is not calculated.

With the sum of all the areas in the table we obtain the volume in voxels. For this case, the volume obtained is 1228583 voxels. In the following image we can see the basal volume obtained comparing it with the volumes of the week (1154866) and month (1126295). Also attached the volumes in voxels. We see that in this case there is a decrease in volume but not very noticeable.

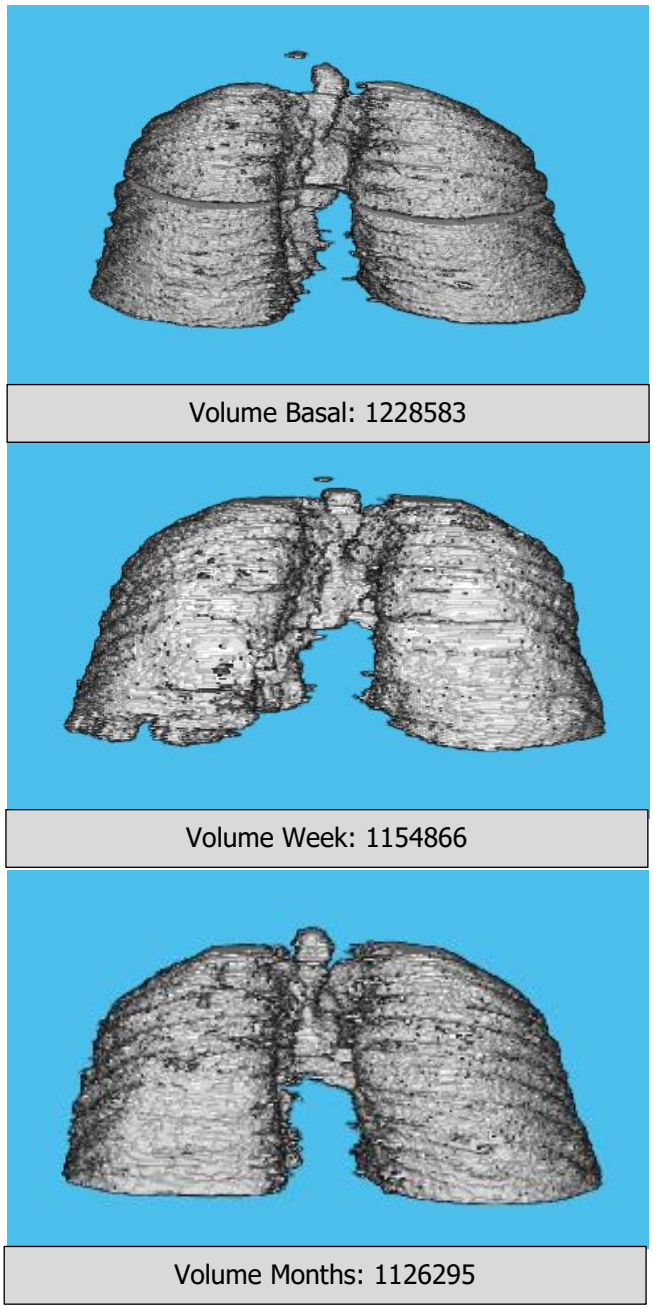

Figure 44 - Basal, week and month volumes obtained

7.2. Anormal CT

We will now analyze an abnormal CT scan for which the patient had to be ruled out for the study. The CT scan is from the patient's week with id 251242. In the following figure we can see the general structure of the CT scan and its central section.

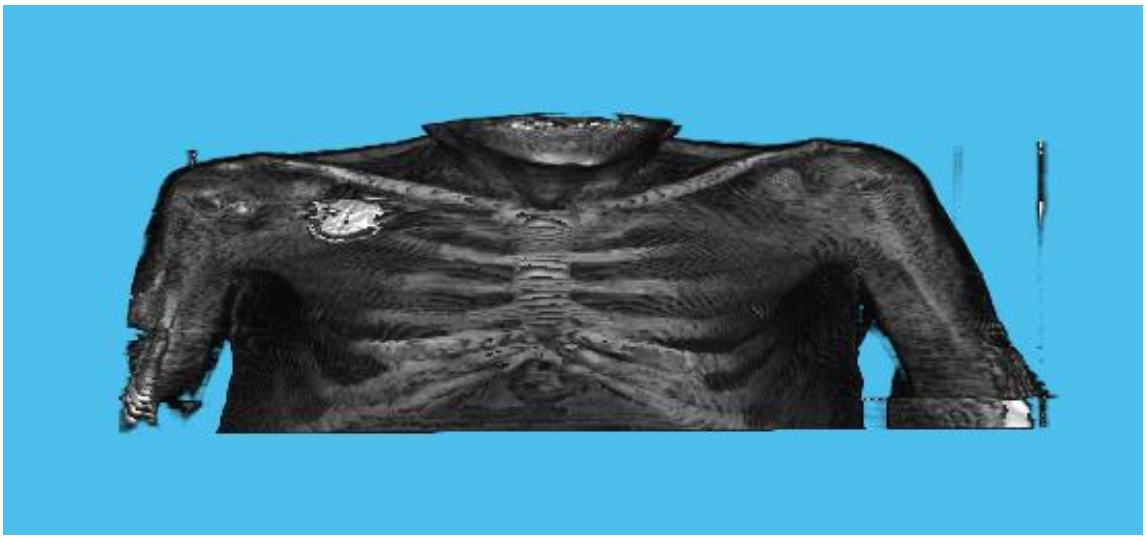

Figure 45 - Structure of the patient with abnormal CT

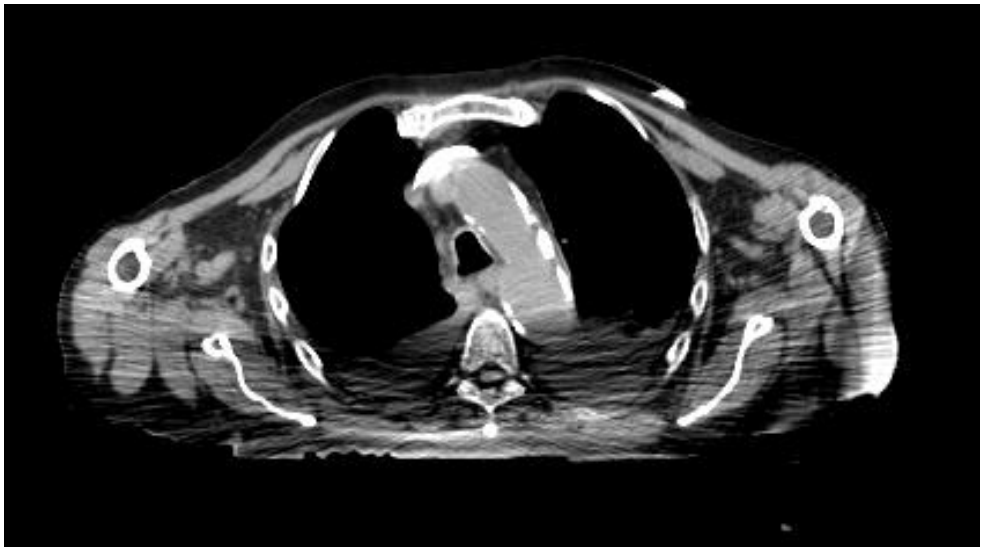

Figure 46 - CT central section of figure 44

From this central section we can see that the CT image is not clear, it has a lot of noise. An attempt was made to process this CT by improving the image in order to obtain more accurate data, since with the current image and the algorithms generated, the results were not adequate. This was not achieved and since it was only a single CT scan of a patient, it was obtained by ruling out this subject.

We will see in the following images the 3D structure of lung volume that we obtain with our algorithm. An example of the central section of the image with its respective mask is also shown to have a better idea of the failure of the algorithm.

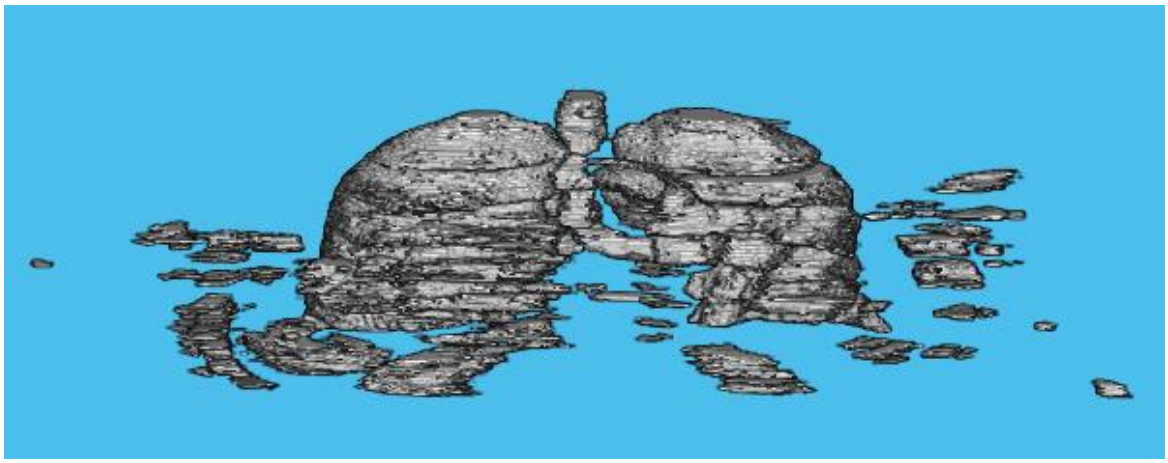

Figure 47 - Lung volume obtained from the CT scan in Figure 44

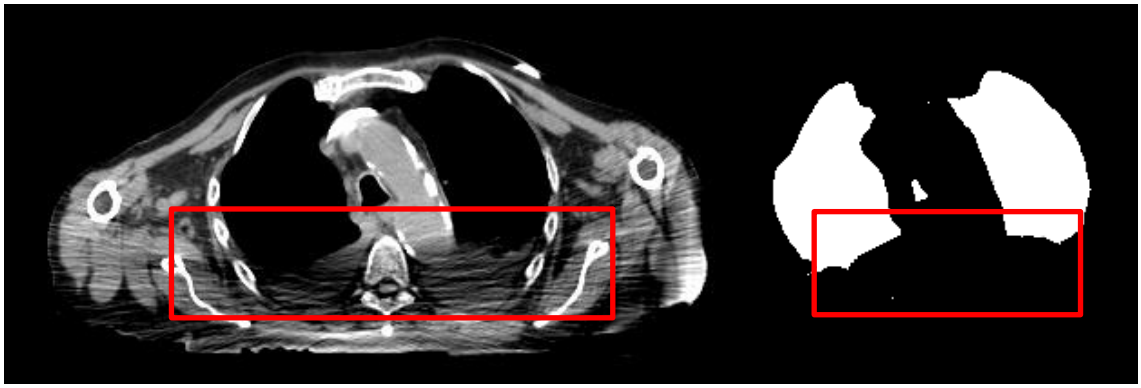

Figure 48 - Example of cutting and applying your CT mask from figure 44

As we can see in the regions highlighted in red, we can see the failure of the algorithm. We see that in the section there is a large area of the lungs that is distorted by the image noise. For this reason, the algorithm is not able to recognize this region as the lung, so an adequate mask is not created.

7.3. URL Algorithms

The two algorithms developed can be found at the following link:

https://github.com/luciasalmerongallar/TFG_Biomedical_Engineering

Within this repository are the functions belonging to the 2D Volume calculation algorithm enhanced with information of the previous CT section along with a folder with the functions of the 3D algorithm.

Bibliography

1. Ge, H., Wang, X., Yuan, X., Xiao, G., Wang, C., Deng, T., Yuan, Q., & Xiao, X. (2020). The epidemiology and clinical information about COVID-19. European journal of clinical microbiology & infectious diseases : official publication of the European Society of Clinical Microbiology, 39(6), 1011–1019. https://doi.org/10.1007/s10096-020-03874-z

2. Siddiqi, H. K., & Mehra, M. R. (2020). COVID-19 illness in native and immunosuppressed states: A clinical-therapeutic staging proposal. The Journal of heart and lung transplantation : the official publication of the International Society for Heart Transplantation, 39(5), 405–407. https://doi.org/10.1016/j.healun.2020.03.012

3. Calabrese, E. J., & Dhawan, G. (2013). How radiotherapy was historically used to treat pneumonia: could it be useful today?. The Yale journal of biology and medicine, 86(4), 555–570.

4. Montero, A., Arenas, M., & Algara, M. (2021). Low-dose radiation therapy: could it be a game-changer for COVID-19?. Clinical & translational oncology : official publication of the Federation of Spanish Oncology Societies and of the National Cancer Institute of Mexico, 23(1), 1–4. https://doi.org/10.1007/s12094-020-02401-y

5. Montero, A., Arenas, M., & Algara, M. (2020) Ongoing trials of low dose raration therapy for covid-19 pneumonia: Studying the past to define the future?. Journal of Clinical Trials. https://www.longdom.org/open-access/ongoing-trials-of-low-dose-radiation-therapy-for-covid19-pneumonia-studying-the-past-to-define-the-future.pdf

6. Arenas, M., Sabater, S., Hernández, V., Rovirosa, A., Lara, P. C., Biete, A., & Panés, J. (2012). Anti-inflammatory effects of low-dose radiotherapy. Indications, dose, and radiobiological mechanisms involved. Strahlentherapie und Onkologie : Organ der Deutschen Rontgengesellschaft ... [et al], 188(11), 975–981. https://doi.org/10.1007/s00066-012-0170-8

7. Huang, C., Wang, Y., Li, X., Ren, L., Zhao, J., Hu, Y., Zhang, L., Fan, G., Xu, J., Gu, X., Cheng, Z., Yu, T., Xia, J., Wei, Y., Wu, W., Xie, X., Yin, W., Li, H., Liu, M., Xiao, Y., … Cao, B. (2020). Clinical features of patients infected with 2019 novel coronavirus in Wuhan, China. Lancet (London, England), 395(10223), 497–506. https://doi.org/10.1016/S0140-6736(20)30183-5

8. Zhu, N., Zhang, D., Wang, W., Li, X., Yang, B., Song, J., Zhao, X., Huang, B., Shi, W., Lu, R., Niu, P., Zhan, F., Ma, X., Wang, D., Xu, W., Wu, G., Gao, G. F., Tan, W., & China Novel Coronavirus Investigating and Research Team (2020). A Novel Coronavirus from Patients with Pneumonia in China, 2019. The New England journal of medicine, 382(8), 727–733. https://doi.org/10.1056/NEJMoa2001017

9. Coronaviridae Study Group of the International Committee on Taxonomy of Viruses (2020). The species Severe acute respiratory syndrome-related coronavirus: classifying 2019-nCoV and naming it SARS-CoV-2. Nature microbiology, 5(4), 536–544. https://doi.org/10.1038/s41564-020-0695-z

10. Dong, E., Du, H., & Gardner, L. (2020). An interactive web-based dashboard to track COVID-19 in real time. The Lancet. Infectious diseases, 20(5), 533–534. https://doi.org/10.1016/S1473-3099(20)30120-1

11. Computed Tomography (CT). (2021). Recuperado 11 de marzo de 2021, de National Institute of Biomedical Imaging and Bioengineering (NIBIB) website: https://www.nibib.nih.gov/science-education/science-topics/computed-tomography-ct

12. Exploraciones con tomografía computarizada (TC) para el cáncer. (2021). Recuperado 11 de marzo de 2021, de National Institute of Biomedical Imaging and Bioengineering (NIBIB) website: https://www.cancer.gov/espanol/cancer/diagnostico-estadificacion/hoja-informativa-tomografia-computarizada

13. Rivera Domínguez, A., de Araujo Martins-Romeo, D., Ruiz García, T., García de la Oliva, A., & Cueto Álvarez, L. (2019). Urgent Multidetector Computed Tomography in Colon Cancer: Postsurgical Changes and Early Complications. Tomografía computarizada multidetector urgente de la cirugía del cáncer colorrectal: Cambios posquirúrgicos y complicaciones tempranas. Radiologia, 61(4), 286–296. https://doi.org/10.1016/j.rx.2019.02.003

14. Exploración TAC de torax. (2021). Recuperado 11 de marzo de 2021, de Radiology Info para pacientes website: https://www.radiologyinfo.org/es/info/chestct

15. The Role of Imaging in Medicine. (2021). Recuperado 11 de marzo de 2021, de Radiology Key website: https://radiologykey.com/the-role-of-imaging-in-medicine/

16. Bercovich, E., & Javitt, M. C. (2018). Medical Imaging: From Roentgen to the Digital Revolution, and Beyond. Rambam Maimonides medical journal, 9(4), e0034. https://doi.org/10.5041/RMMJ.10355

17. Thirumaran, J., & Shylaja, S. (2015). Medical Image Processing – An Introduction Dr.

18. MATLAB. (2010). version 7.10.0 (R2010a). Natick, Massachusetts: The MathWorks Inc.

19. Key Concepts. (2021). Recuperado 11 de marzo de 2021, de DICOM strandard website: https://www.dicomstandard.org/concepts

20. Mildenberger, P., Eichelberg, M., & Martin, E. (2002). Introduction to the DICOM standard. European radiology, 12(4), 920–927. https://doi.org/10.1007/s003300101100